

UC Davis

UC Davis Previously Published Works

Title

The Nesprin-1/-2 ortholog ANC-1 regulates organelle positioning in *C. elegans* independently from its KASH or actin-binding domains

Permalink

<https://escholarship.org/uc/item/9ns3187p>

Authors

Hao, Hongyan
Kalra, Shilpi
Jameson, Laura E
[et al.](#)

Publication Date

2021

DOI

10.7554/elife.61069

Peer reviewed

The Nesprin-1/-2 ortholog ANC-1 regulates organelle positioning in *C. elegans* independently from its KASH or actin-binding domains

Hongyan Hao, Shilpi Kalra, Laura E Jameson, Leslie A Guerrero, Natalie E Cain, Jessica Bolivar, Daniel A Starr*

Department of Molecular and Cellular Biology, University of California, Davis, Davis, United States

Abstract KASH proteins in the outer nuclear membrane comprise the cytoplasmic half of linker of nucleoskeleton and cytoskeleton (LINC) complexes that connect nuclei to the cytoskeleton. *Caenorhabditis elegans* ANC-1, an ortholog of Nesprin-1/2, contains actin-binding and KASH domains at opposite ends of a long spectrin-like region. Deletion of either the KASH or calponin homology (CH) domains does not completely disrupt nuclear positioning, suggesting neither KASH nor CH domains are essential. Deletions in the spectrin-like region of ANC-1 led to significant defects, but only recapitulated the null phenotype in combination with mutations in the transmembrane (TM) span. In *anc-1* mutants, the endoplasmic reticulum ER, mitochondria, and lipid droplets were unanchored, moving throughout the cytoplasm. The data presented here support a cytoplasmic integrity model where ANC-1 localizes to the ER membrane and extends into the cytoplasm to position nuclei, ER, mitochondria, and other organelles in place.

Introduction

Cellular organization is an essential process. Organelles are interconnected and mostly constrained to specific subcellular locations when they are not actively transported longer distances by cytoskeletal motor proteins (*van Bergeijk et al., 2016*). For example, nuclear positioning is essential for a wide variety of cellular and developmental processes, including fertilization, cell division, cell polarization, gametogenesis, central-nervous system development, and skeletal muscle function (*Bone and Starr, 2016; Gundersen and Worman, 2013*). Defects in nuclear positioning are associated with multiple neuromuscular diseases (*Calvi and Burke, 2015; Folker and Baylies, 2013; Gundersen and Worman, 2013*). Furthermore, the Golgi apparatus and centrosomes are often found next to the nucleus, while the ER and mitochondria are usually spread throughout the cell (*van Bergeijk et al., 2016*). The cellular tensegrity model posits that organelles are physically coupled to the cytoskeleton, plasma membrane, and extracellular matrix so that the cell acts as a single mechanical unit (*Jaalouk and Lammerding, 2009; Wang et al., 2009*). The mechanisms that maintain cellular tensegrity and how it relates to organelle positioning are poorly understood, especially in vivo.

Nuclei are connected to the rest of the cell by LINC (linker of nucleoskeleton and cytoskeleton) complexes. SUN (Sad-1/UNC-84) proteins integral to the inner nuclear membrane and KASH (Klar-sicht, ANC-1, and SYNE homology) proteins that span the outer nuclear membrane interact with each other in the perinuclear space to form LINC complexes. The cytoplasmic domains of KASH proteins interact with various components of the cytoskeleton (*Luxton and Starr, 2014*), while the nucleoplasmic domains of SUN proteins interact with lamins. Thus, LINC complexes bridge the

*For correspondence:
dastarr@ucdavis.edu

Competing interests: The authors declare that no competing interests exist.

Funding: See page 26

Received: 14 July 2020
Accepted: 11 April 2021
Published: 16 April 2021

Reviewing editor: Maddy Parsons, King's College London, United Kingdom

© Copyright Hao et al. This article is distributed under the terms of the [Creative Commons Attribution License](https://creativecommons.org/licenses/by/4.0/), which permits unrestricted use and redistribution provided that the original author and source are credited.

nuclear envelope and mechanically couple the nucleoskeleton to the cytoskeleton (**Chang et al., 2015; Lee and Burke, 2018; Starr and Fridolfsson, 2010**). LINC complex inhibition reduces the stiffness and increases the deformability of the entire cytoplasm in mammalian tissue culture cells, even far from the nuclear envelope and beyond the predicted reach of LINC complexes (**Gill et al., 2019; Stewart-Hutchinson et al., 2008**). Whether LINC complexes maintain the mechanical properties of the cytoplasm in vivo is relatively unexplored.

Here, we investigate the role of LINC complexes with giant KASH proteins in organelle positioning in *Caenorhabditis elegans*. Most of the hypodermis of an adult *C. elegans* consists of a giant syncytium, the hyp7, containing 139 evenly-spaced nuclei that are anchored in place (**Altun and Hall, 2009**). Furthermore, *C. elegans* have invariant developmental lineages, are optically clear, and are easily genetically manipulated, making the hyp7 an ideal in vivo model to study organelle positioning. A LINC complex made of the KASH protein ANC-1 and the SUN protein UNC-84 is responsible for nuclear anchorage in *C. elegans* (**Starr, 2019**). UNC-84 is a canonical SUN protein that is orthologous to mammalian SUN1 and SUN2 and is the only known SUN protein in postembryonic somatic tissues in *C. elegans* with a nucleoplasmic domain that interacts directly with the lamin protein LMN-1 (**Bone et al., 2014**). ANC-1 is an exceptionally large protein of up to 8545 residues with two tandem calponin homology (CH) domains at its N terminus and a KASH domain at its C terminus (**Starr and Han, 2002**). ANC-1 orthologs *Drosophila* MSP-300 and mammalian Nesprin-1 Giant (G) and -2G have similar domain arrangements (**Starr and Fridolfsson, 2010**). Unlike MSP-300, Nesprin-1G, and -2G, which each contains greater than 50 spectrin-like repeats, ANC-1 consists of six tandem repeats (RPs) of 903 residues that are almost 100% conserved with each other at the nucleotide level (**Liem, 2016; Rajgor and Shanahan, 2013; Starr and Han, 2002; Zhang et al., 2001**). While spectrin-like repeats have not been identified in the ANC-1 RPs, most of ANC-1 is predicted to be highly helical, like spectrin (**Starr and Han, 2002**). The CH domains of ANC-1 interact with actin filaments in vitro and co-localize with actin structures in vivo, while the KASH domain of ANC-1 requires UNC-84 for its localization to the outer nuclear membrane (**Starr and Han, 2002**). UNC-84 is thought to interact with lamins to connect LINC to the nucleoskeleton while ANC-1 extends away from the outer nuclear membrane into the cytoplasm to tether nuclei to actin filaments (**Starr and Han, 2002**).

Evidence from multiple systems suggests that giant KASH orthologs might not solely function as nuclear tethers. We have observed that hyp7 syncytia in *anc-1* null animals display a stronger nuclear positioning defect than *unc-84* null animals (**Cain et al., 2018; Jahed et al., 2019**) and mitochondria are unanchored in *anc-1*, but not in *unc-84* mutants (**Starr and Han, 2002**). These results suggest that ANC-1 has LINC complex-independent roles for anchoring nuclei and mitochondria. Likewise, mitochondria and the ER are mispositioned in *Drosophila msp-300* mutant muscles (**Elhanany-Tamir et al., 2012**). Finally, it remains to be determined if the CH domains of ANC-1 are necessary for nuclear anchorage. Mouse Nesprin-1 and -2 have isoforms lacking CH domains (**Duong et al., 2014; Holt et al., 2016**) and Nesprin-1 CH domains are dispensable for nuclear positioning during mouse skeletal muscle development (**Stroud et al., 2017**).

To address these ambiguities, we use ANC-1 to examine how giant KASH proteins position nuclei and other organelles. We find that for nuclear anchorage, the ANC-1 KASH domain plays a relatively minor role, and the CH domains are dispensable. Rather, multiple large cytoplasmic domains and the C-terminal transmembrane (TM) span of ANC-1 are required for nuclear anchorage. Moreover, in *anc-1* null mutants, the entire cytoplasm is disorganized, and the ER is unanchored and moves freely throughout the cytoplasm. Together, our results support a model in which ANC-1 associates with ER membranes to regulate the mechanical properties of the cytoplasm, thereby anchoring nuclei, mitochondria, ER, and other organelles.

Results

ANC-1 promotes proper nuclear anchorage through a LINC complex-independent mechanism

Loss-of-function mutations in *anc-1* disrupt the even spacing of hyp7 syncytial nuclei (**Cain et al., 2018; Starr and Han, 2002**). We use the number of nuclei in contact with each other as a metric for hyp7 nuclear anchorage defects (**Cain et al., 2018; Fridolfsson et al., 2018**). In wild type

(WT) animals, very few hyp7 nuclei were touching. In contrast, over 50% of hyp7 nuclei were clustered with at least one other nucleus in *anc-1(e1873)* null mutants. Significantly fewer hyp7 nuclei were unanchored in *unc-84(n369)* null mutants (**Figure 1C**). This trend was also observed in adult syncytial seam cells (**Figure 1—figure supplement 1**). Throughout this manuscript, we call nuclear anchorage defects that are statistically similar to *anc-1* null mutants as severe, defects statistically similar to *unc-84* null mutants but still significantly worse than wild type as mild, and defects statistically between *anc-1* and *unc-84* null mutants as intermediate.

The greater severity of the nuclear anchorage defect in *anc-1* null mutants compared to *unc-84* suggests that ANC-1 plays additional roles in nuclear positioning independently of its SUN partner UNC-84. We used CRISPR/Cas9 gene editing to delete the luminal peptides of the ANC-1 KASH domain (**Figure 1D**). We predicted the *anc-1(ΔKASH)* mutants would abrogate the interaction between ANC-1 and UNC-84 and phenocopy *unc-84(null)* animals. Two independent *anc-1(ΔKASH)* mutants exhibited mild nuclear anchorage defects similar to those observed in *unc-84(null)* mutants (**Figure 1B–C**). Together, these results suggest that the SUN/KASH interaction only partially contributes to nuclear anchorage, implicating the large cytoplasmic domain of ANC-1 as the major player in nuclear positioning.

The ANC-1 N-terminal CH domains are not required for hyp7 nuclear positioning

We next deleted the CH domains at the N terminus of the largest isoforms of ANC-1, which are predicted to interact with actin, and replaced them with GFP using CRISPR/Cas9 gene editing. Hyp7 nuclei did not cluster in *anc-1(ΔCH)* mutants (**Figure 2B**). Thus, the CH domains of ANC-1 are not required for hyp7 nuclear anchorage.

Nesprin-1 and -2 have multiple splice isoforms, many of which are missing the CH domains (**Rajgor et al., 2012; Stroud et al., 2017**). We hypothesized a shorter *anc-1* isoform lacking the CH domains would be sufficient for nuclear anchorage. RNAseq and expressed sequence tag data published on WormBase (**Harris et al., 2020**) suggest that *anc-1* has at least three isoforms (**Figure 2A**). We tested whether a shorter isoform lacking CH domains, *anc-1b*, is sufficient for hyp7 nuclear anchorage. RNAi constructs targeting the 5' exons specific to the *anc-1a/c* long isoforms did not cause nuclear anchorage defects (**Figure 2A–B**). However, RNAi targeting a repetitive region in all three predicted isoforms caused severe nuclear anchorage defects (**Figure 2A–B**). We also analyzed four nonsense mutations. Alleles that are predicted to disrupt the longer *anc-1a/c* isoforms but not the shorter *anc-1b* isoform, *anc-1(W427*)*, and *anc-1(W621*)* were normal for nuclear anchorage. In contrast, both *anc-1(Q1603*)* and *anc-1(Q2878*)* alleles, which are predicted to add premature stop codons to all three predicted isoforms, led to severe nuclear anchorage defects (**Figure 2A–B**). These results suggest that the shorter *anc-1b* isoform lacking the CH domains is sufficient for nuclear anchorage.

We next tested whether *anc-1b* is expressed in hyp7. First, 5' RACE (Rapid amplification of cDNA ends) was used to identify the start of the *anc-1b* predicted transcript (**Figure 2C**). The RACE product contained an SL1 sequence at its 5' end, suggesting this represents the end of a bona fide transcript (**Figure 2D**). To test if the *anc-1b* isoform is expressed in hyp7, we fused the *anc-1b* promoter and ATG to an *nls::gfp::lacZ* reporter and expressed it in transgenic animals. The *anc-1b* promoter drove GFP expression in hyp7 (**Figure 2E**, yellow arrows). Taken together, these results suggest the conserved CH domains are not necessary for hyp7 nuclear anchorage and the *anc-1b* isoform expressed in the hypodermis plays a major role in hyp7 nuclear anchorage.

Spectrin-like domains of ANC-1b are required for nuclear anchorage

We predicted that the six tandem repeats (RPs) of ANC-1 function analogously to the spectrin-like domains of Nesprin-1 and -2. We modeled the structure of pieces of the ANC-1 RPs using the protein-folding prediction software QUARK (**Xu and Zhang, 2012; Xu and Zhang, 2013**) and found that they are predicted to form helical bundles remarkably similar to the structure of spectrin (**Figure 3A,D; Grum et al., 1999**), suggesting the tandem repeats are analogous to spectrin-like domains.

We next tested the necessity of the ANC-1 spectrin-like repeats and the neighboring cytoplasmic domains for nuclear anchorage by making in-frame deletions of portions of *anc-1* using CRISPR/

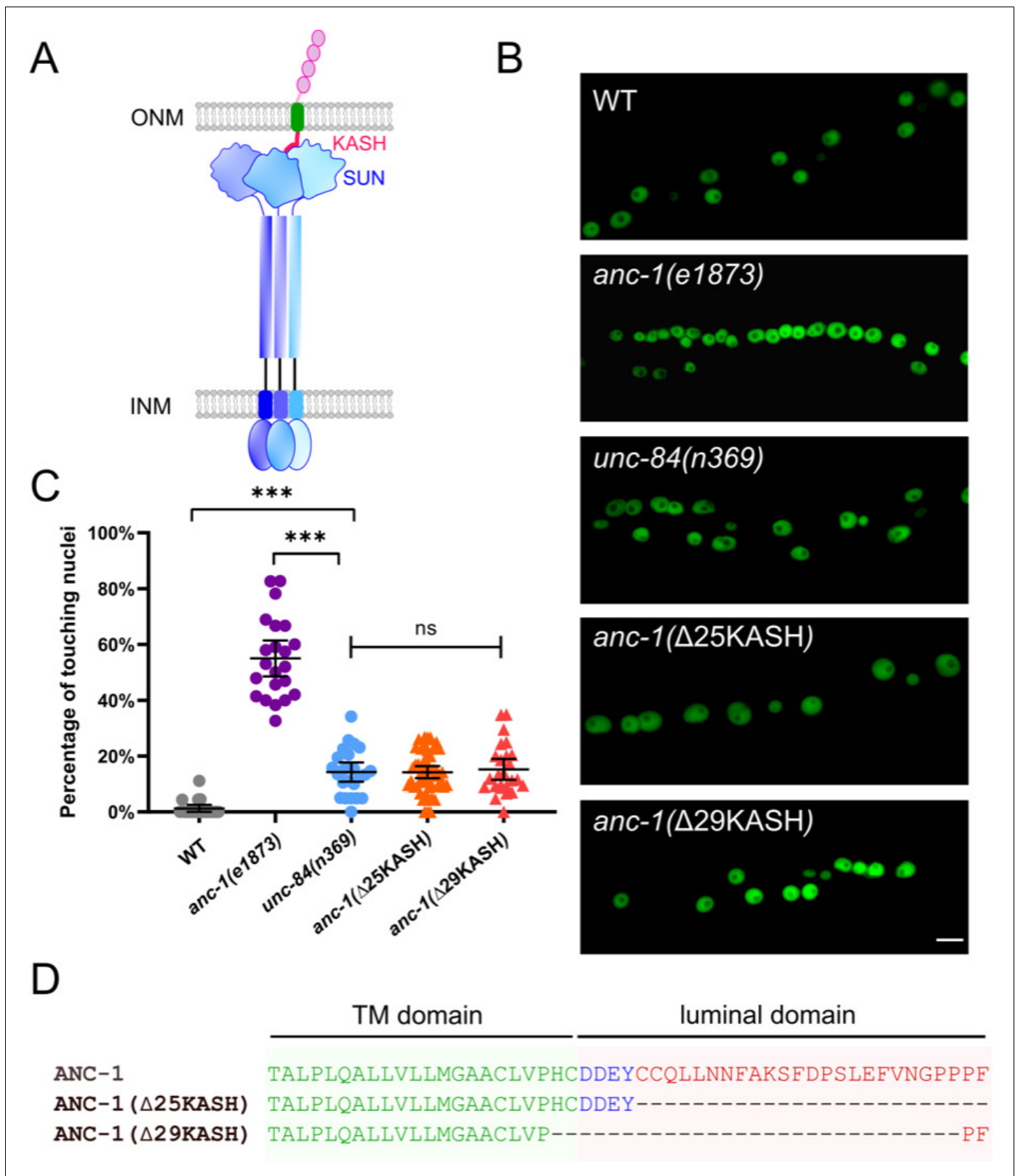


Figure 1. ANC-1 has a linker of nucleoskeleton and cytoskeleton (LINC) complex-independent role in anchoring nuclei. (A) Model of the LINC complex. Trimers of the SUN protein UNC-84 (purple and blue) and the KASH protein ANC-1 (red, green, and pink, only one of the trimers is shown) form the LINC complex, which spans the outer nuclear membrane (ONM) and inner nuclear membrane (INM). (B) Lateral views of adult *C. elegans* expressing hypodermal nuclear GFP in wild type (WT) or indicated mutants. Scale bar, 10 μ m. (C) Quantification of nuclear anchorage defects. Each point

Figure 1 continued on next page

Figure 1 continued

represents the percentage of touching nuclei on one side of a young adult animal. Means with 95% CI error bars are shown. ANOVA and Tukey's multiple comparisons tests were used for statistical analysis; ns means not significant, $p > 0.05$; *** $p \leq 0.001$. $n \geq 20$ for each strain. (D) Sequences of the transmembrane (TM) domain and the luminal domain of ANC-1 showing the deletions analyzed.

The online version of this article includes the following figure supplement(s) for figure 1:

Figure supplement 1. Nuclear anchorage defects in seam cell syncytia.

Cas9-mediated gene editing. The N-terminal fragment 1 (F1) contains 1969 residues of ANC-1b from the start codon to the start of the RPs and fragment 2 (F2) contains the 277 residues between the RPs and the C-terminal transmembrane span (Figure 3A). The deletion of the F1 domain or all six RPs caused intermediate nuclear anchorage defects (Figure 3B–C). ANC-1b with only one of the normal six repeats had an intermediate nuclear anchorage defect that was significantly greater than in wild type but not as severe as the *anc-1*(Δ 6RPS) mutant (Figure 3C). In contrast, the *anc-1*(Δ F2) mutant had no nuclear anchorage defect (Figure 3C). Since the *anc-1*(Δ 6RPS) and *anc-1*(Δ F1) defects were less severe than *anc-1* null alleles, we made double mutants with *unc-84*(n369) to see if mutations in the cytoplasmic portions of ANC-1 were synergistic with mutations in the KASH domain. Both *anc-1*(Δ F1); *unc-84*(n369) and *anc-1*(Δ 6RPS); *unc-84*(n369) double mutants significantly enhanced the nuclear anchorage defects of the single mutations (Figure 3C). However, the hyp7 nuclear anchorage defects in *anc-1*(Δ F1); *unc-84*(n369) and *anc-1*(Δ 6RPS); *unc-84*(n369) double mutants were still less severe than *anc-1*(e1873) null mutants, suggesting that multiple parts of ANC-1b mediate proper hyp7 nuclear positioning (Figure 3C). Together, these results indicate that (1) F1 and the RPs play roles in nuclear anchorage, (2) multiple repeats are necessary for normal function, and (3) the F2 region is dispensable for hyp7 nuclear positioning.

The ER is unanchored in *anc-1* mutants

In addition to nuclear positioning, ANC-1 functions in mitochondria distribution and morphology in the hypodermis and muscle cells (Hedgecock and Thomson, 1982; Starr and Han, 2002). We therefore asked if ANC-1 also anchors other organelles. We characterized the ER in live hyp7 syncytia of *anc-1* and *unc-84* mutants using a single-copy GFP::KDEL marker (*pw5i83*; gift of Barth Grant). In wild type, the ER formed a network evenly distributed throughout hyp7 (Figure 4A). We used blind scoring to classify single images of each animal's ER as normal (evenly distributed in what appeared to be sheets), mild defects (lots of sheet-like structures, but occasionally not uniformly spread throughout the syncytium), strong defects (considerable mispositioning and clustering of ER, but still in large units), or severe defects (complete mispositioning and extensive fragmenting of the ER) (Figure 4 and Figure 4—figure supplement 1). About a third of wild type adults had normally distributed ER, while the rest had mild ER positioning defects, perhaps due to the pressure on the worm from the coverslip (Figure 4A–B). However, ER networks in *anc-1* null mutants were severely disrupted and often fragmented (Figure 4A–B). We also observed the dynamics of the ER in live animals. In wild type animals, the hypodermal ER was anchored as an interconnected network and exhibited limited motion while the animal crawled (Figure 4C,E–F, Video 1). However, in *anc-1* null mutants, ER fragments drifted apart and often formed large aggregates, suggesting that the anchorage of the ER network was disrupted (Figure 4D–F, Video 2). To quantify this phenotype, we measured the change in distance between distinct points over time. In wild type, the average distance change between parts of the ER was less than 1 μ m per second, whereas in *anc-1* mutants, the average change in distance more than doubled (Figure 4E), suggesting that the ER had lost its overall interconnectivity and that fragments were unanchored from the rest of the ER.

We next examined whether UNC-84 is required for ER positioning. Still images of *unc-84*(n369) null mutants scored blindly were similar to wild type ER (Figure 4A–B). However, in some videos of *unc-84*(n369) mutants, there were slight changes in the organization of the ER over time (Video 3), suggesting that *unc-84* null mutants had a minor ER positioning defect. Most *anc-1*(Δ 29KASH) mutants had mild defects in ER positioning, and only about a quarter had more severe defects, significantly less than *anc-1*(e1873) null mutants. In contrast, more than 80% of *anc-1*(Δ 6RPS) animals had strong or severe ER positioning defects, similar to *anc-1* null mutants (Figure 4A–B). These

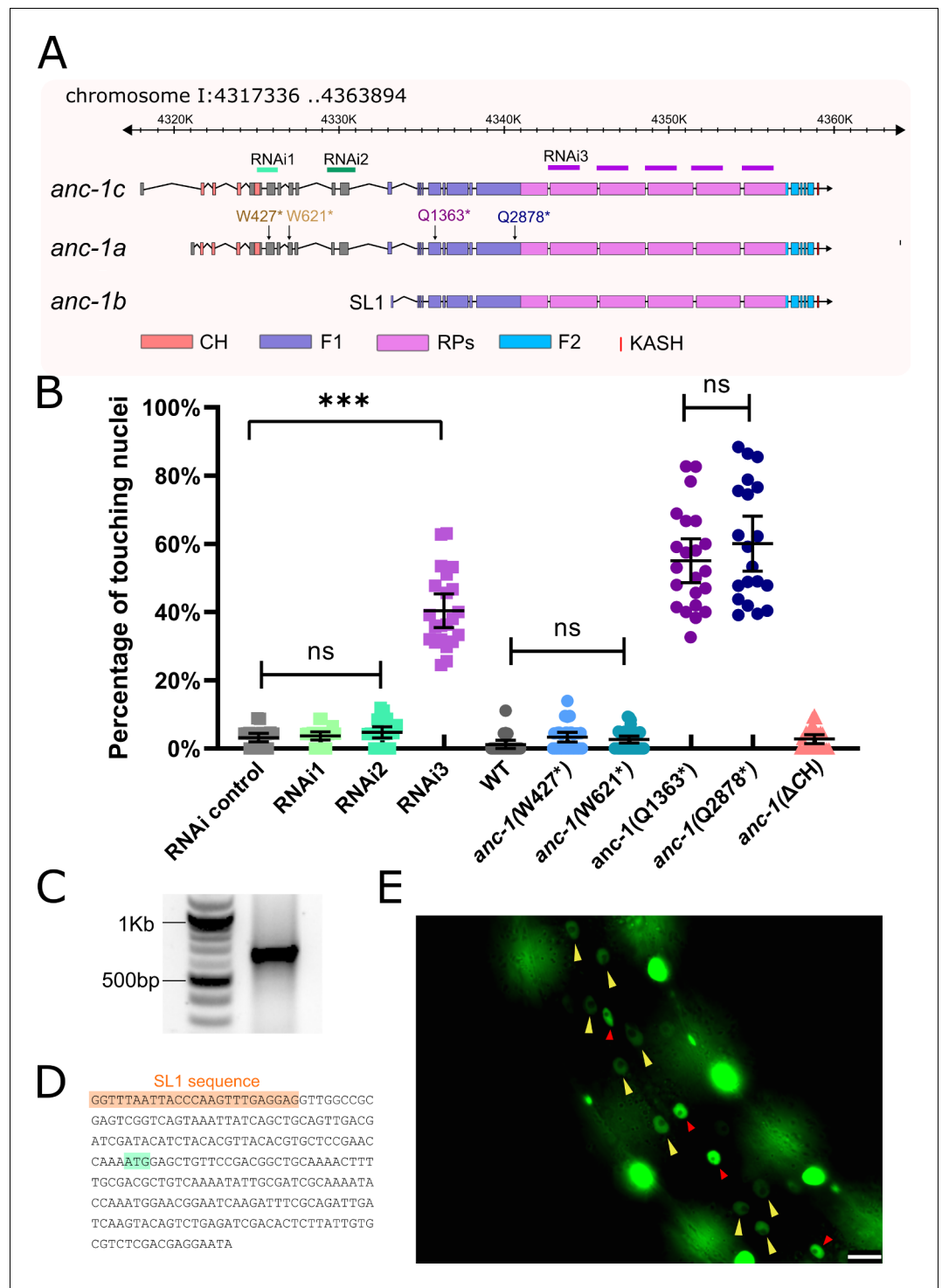


Figure 2. *anc-1b* is the major isoform in *hyp7* nuclear anchorage. (A) Schematic gene structure of *anc-1a*, *b*, and *c* isoforms (modified from the J-Brower in Wormbase). Domains are color-coded. CH = calponin homology; F1 = fragment one from the ATG of ANC-1b to the beginning of the repeats; RPs = the six exact repeats of about 900 residues each; F2 = fragment two from the end of the repeats to the transmembrane (TM) span; WT = wild type; and KASH = Klarsicht, ANC-1, Syne homology, in this case referring to the residues in the lumen of the nuclear envelope. The target regions of RNAi constructs are labeled. Premature stop mutations are indicated using the numbering the *anc-1a* isoform. (B) Quantification of nuclear anchorage defects in *anc-1* mutant and RNAi animals. Means with 95% CI are shown in the graph. ANOVA and Tukey's multiple comparisons tests were used for statistical analysis. ns, not significant, $p > 0.05$; *** $p \leq 0.001$. $n \geq 20$ for each strain. (C) An agarose gel showing Figure 2 continued on next page

Figure 2 continued

the 5'-RACE products on the right lane. (D) Partial sequence of the 5'-RACE product. An SL1 sequence (orange) adjacent to the 5' end of the *anc-1b* transcript was identified. The predicted start codon is in light green. (E) Lateral view of a worm showing the expression of nls::GFP driven by *anc-1b* promoter. Yellow arrows mark hyp7 nuclei; the red arrows mark seam cell nuclei; and the bright, unmarked nuclei are in muscle cells. Scale bar, 10 μ m.

results indicated that ANC-1 is essential for ER positioning through mostly LINC complex-independent mechanisms.

ANC-1 localizes to ER membranes

Since ANC-1 functions, in part, independently of LINC complexes at the nuclear envelope and because ANC-1 regulates ER positioning, we hypothesized that ANC-1 localizes to multiple membranes, including those away from the nuclear envelope. To study the localization of ANC-1, we tagged endogenous ANC-1 with GFP using CRISPR/Cas9 gene editing. The tag was placed either at the N-terminus of ANC-1b, or between the six tandem RPs and the F2 region to see if the opposite ends of ANC-1 localize to different structures (Figure 5A). Both strains were nearly wild type for hyp7 nuclear positioning (Figure 5B). Both GFP::ANC-1b and ANC-1::GFP::F2 localized in similar

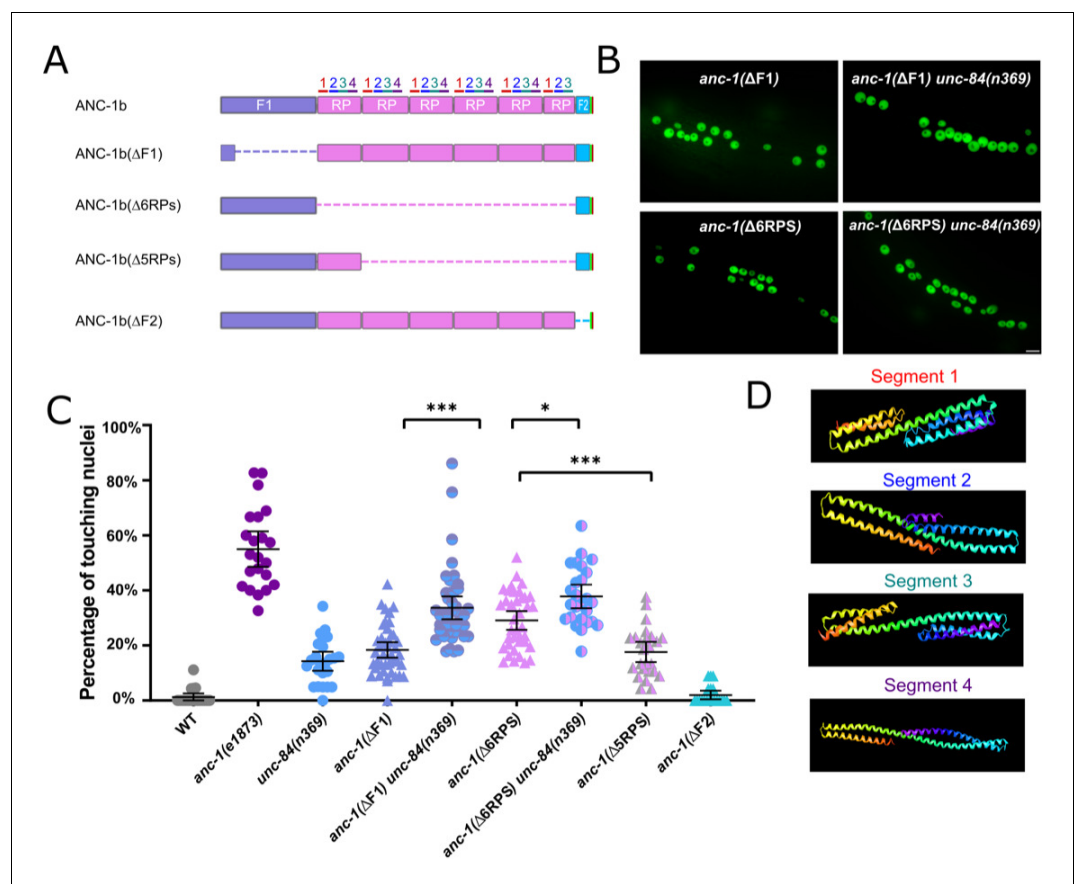


Figure 3. Cytoplasmic domain deletion analysis of ANC-1b. (A) Schematics of the ANC-1b cytoplasmic domain deletions. (B) Lateral views are shown of young adult *C. elegans* expressing hypodermal nuclear GFP in the indicated genotypes. Scale bar, 10 μ m. (C) Quantification of nuclear anchorage in the wild type (WT) as well as *anc-1b* domain deletion mutants. Each point represents the percentage of touching nuclei on one side of a young adult animal. Means with 95% CI error bars are shown. ANOVA and Tukey's multiple comparisons tests were used for statistical analysis. * $p \leq 0.05$; ** $p \leq 0.01$; *** $p \leq 0.001$. $n \geq 20$ for each strain. The data in the first three columns, WT, *anc-1*(e1873), and *unc-84*(n369) are duplicated from Figure 1C and copied here for easy reference. (D) QUARK result for three fragments in the tandem repeats (RPs). The positions of the fragments are indicated in 3A.

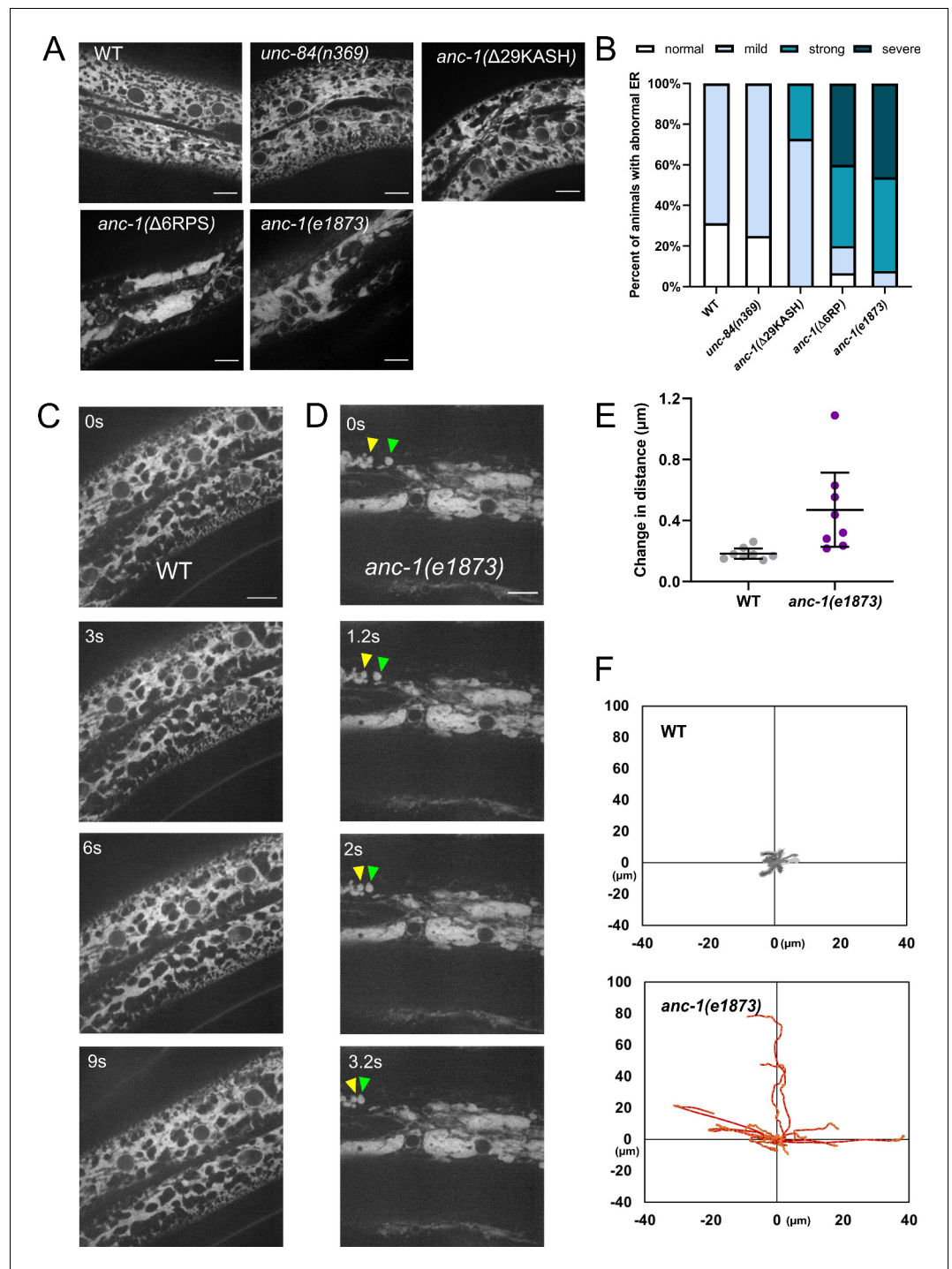


Figure 4. The ER is mispositioned in *anc-1* mutants. (A) Representative images of the hyp7 ER labeled with the GFP::KDEL marker in the young adult animals. (B) Scoring of the ER positioning defects. ER images of the listed strains were mixed and randomized for blind analysis by multiple researchers. $n \geq 11$ for each strain. (C–D) Time-lapse images of hyp7 GFP::KDEL marker (C) over 9 s in wild type (WT) or (D) over 3.2 s in *anc-1* null. Arrowheads show two fragments of ER that changed their relative distance from one another over a short period of time. (E–F) To quantify ER displacement, three spots on each WT and *anc-1(e1873)* movie were tracked. The average change in distance between two points in 200 ms intervals is plotted in (E). The trajectories of the relative movements of each spot apart from the others are shown in (F). Eight movies of each strain were analyzed. Scale bar, 10 μm for all the images.

The online version of this article includes the following figure supplement(s) for figure 4:

Figure 4 continued on next page

Figure 4 continued

Figure supplement 1. Raw data for ER morphology assays.

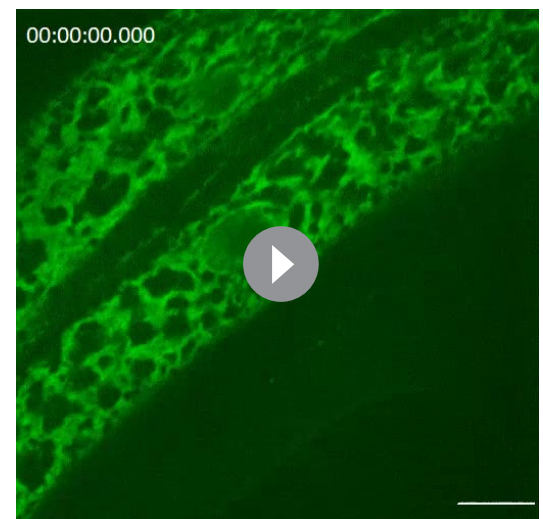
patterns throughout the cytoplasm of adult *hyp7* syncytia (**Figure 5C–D**). To examine the localization of the ANC-1b isoform alone, we introduced a premature stop codon mutation to disrupt the longer *anc-1a* and *c* isoforms in the GFP::ANC-1b strain, which did not significantly change GFP::ANC-1b localization (**Figure 5E**). These data are consistent with our model that *anc-1b* plays the major role in *hyp7* nuclear positioning.

We next examined whether the cytoplasmic domains of ANC-1b are required for localization. Deletion of the F1 domain did not dramatically change localization of GFP::ANC-1b (**Figure 5F**). However, deletion of the six tandem repeats enriched GFP::ANC-1b around the nuclear envelope (**Figure 5G**), as did the deletion of five of the six repeats (**Figure 5H**). However, the intensity of the six repeat deletion mutant is significantly less than wild type GFP::ANC-1b (**Figure 5—figure supplement 1**), making it possible that the phenotype is due to less ANC-1 being present. Yet, the deletion mutant is significantly enriched at the nuclear envelope (**Figure 5—figure supplement 1B–C**), supporting the hypothesis that the defect is due to a loss of ANC-1 repeats at the general ER. The nuclear envelope enrichment of GFP::ANC-1b(Δ 5RPs) was not observed when *unc-84* was mutated (**Figure 5I**), suggesting the nuclear envelope enrichment of GFP::ANC-1b is UNC-84-dependent.

The ANC-1 localization pattern in **Figure 6** is consistent with a model where ANC-1 localizes to ER membranes. In this model, a construct containing the transmembrane span near the C-terminus of ANC-1 but lacking the C-terminal, luminal part of the KASH domain would be sufficient for ER localization. Deletion of both the transmembrane span and the luminal parts of KASH with CRISPR/Cas9 resulted in a significantly worse nuclear anchorage defect than deleting only the luminal KASH domain (**Figure 6B**). Similarly, ER positioning defects were worse in *anc-1*(Δ TK) than in *anc-1*(Δ 25KASH) animals (**Figure 6C**). We next examined the role of the neck region, which is located immediately adjacent to the cytoplasmic side of the transmembrane span. When GFP was knocked-in between the neck region and the transmembrane span to make *anc-1*(*yc36[anc-1::gfp3Xflag::kash]*), it caused a significant nuclear anchorage defect (**Figure 6A–B**). Moreover, extending the deletion in *anc-1*(Δ F2), which had no *hyp7* nuclear anchorage defect (**Figure 3C**), an additional nine residues to remove the neck, caused a significant nuclear anchorage defect (**Figure 6A–B**). This suggests that the neck region next to the transmembrane span of ANC-1 plays a role in nuclear positioning, perhaps by targeting the C-terminus of ANC-1 to a membrane.

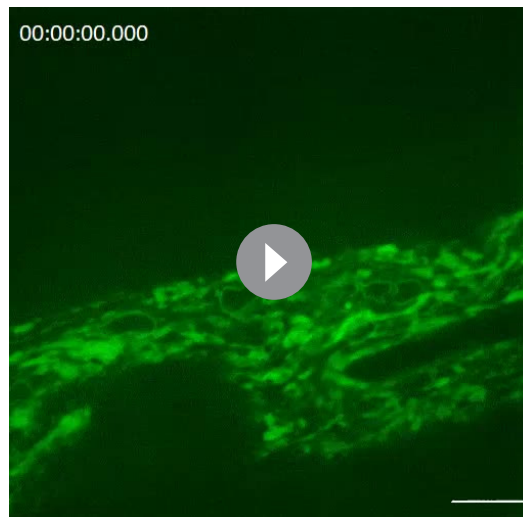
As shown above, a double mutant that lacks both the ANC-1 repeat region and LINC complex function in the form of an *unc-84*(null) had an intermediate defect (**Figure 3B**). This suggests that a third domain of ANC-1, in addition to the luminal portions of KASH and the RPs, is involved in positioning nuclei. To test this hypothesis, we made an *anc-1*(*gfp::anc-1b:: Δ 6rps:: Δ tk*) mutant line and found that it had a severe nuclear anchorage defect that was not significantly different from the *anc-1*(*e1873*) null mutant (**Figure 6B**). Together, these data support a model in which the transmembrane span is important for targeting ANC-1 to the ER/nuclear envelope membrane where ANC-1 then positions the ER and nuclei via LINC complex-independent mechanisms.

To further examine the role of the transmembrane span in ER and nuclear positioning, we



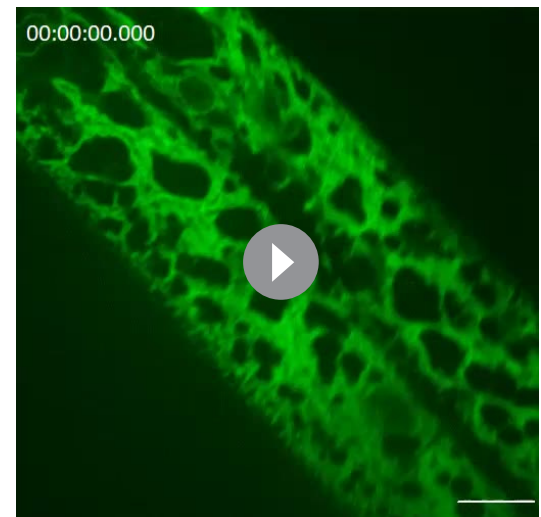
Video 1. The ER is anchored in wild type (WT) *hyp7*. An example video of the *hyp7* ER in young adult wild type *C. elegans* expressing *pwSi83[p_{hyp7}gfp::kdel]*. Images were captured at the interval of 0.2 s for 10 s. Scale bar, 10 μ m.

<https://elifesciences.org/articles/61069#video1>



Video 2. The ER is unanchored in *anc-1(e1873)* mutant hyp7. An example video of the hyp7 ER in the young adult *anc-1(e1873)* mutant *C. elegans* expressing *pwSi83[p_{hyp7}:gfp::kdel]*. Images were captured at the interval of 0.2 s for 10 s. Scale bar, 10 μ m.

<https://elifesciences.org/articles/61069#video2>



Video 3. ER positioning in *unc-84(null)* mutant hyp7. An example of one of the most severe ER positioning defects observed is shown in a video of the hyp7 ER in the young adult *unc-84(n369)* mutant *C. elegans* expressing *pwSi83[p_{hyp7}:gfp::kdel]*. Images were captured at the interval of 0.25 s for 4 s. Scale bar, 10 μ m.

<https://elifesciences.org/articles/61069#video3>

observed the co-localization of ANC-1 with an ER membrane marker (**Figure 7**). A single-copy hypodermal-specific mKate2::TRAM-1 ER marker strain (Rolls *et al.*, 2002) was generated and crossed with GFP::ANC-1b. The wild type GFP::ANC-1b fusion protein localized similarly to the ER marked by mKate2::TRAM-1 (**Figure 7A**). We used the ImageJ plug-in ScatterJ to quantify the co-localization and the Pearson's correlation coefficient averaged from 17 images (**Figure 7G**). Our second GFP construct, ANC-1::GFP::F2, also co-localized with the ER (**Figure 7B,G**). Similar results were obtained when co-localizing mKate2::ANC-1b and GFP::KDEL, but since the GFP::KDEL was overexpressed and significantly brighter than the mKate2::ANC-1b, we only present the analyses with GFP ANC-1 fusion proteins co-localizing with mKate2::TRAM-1, which is expressed at lower levels from a single-copy transgene. In contrast, GFP::ANC-1b did not co-localize with lipid droplets or mitochondria (**Figure 7—figure supplement 1**).

Deleting the luminal portion of the KASH domain from GFP::ANC-1b (GFP::ANC-1b:: Δ KASH) did not significantly change its localization pattern relative to the wild type construct (**Figure 7C,G**). In contrast, deletion of both the luminal KASH peptide and the transmembrane span (GFP::ANC-1b:: Δ TK) resulted in many cases where GFP::ANC-1b:: Δ TK almost normally localized to the ER (**Figure 7D,G**) while in other animals it localized in parts of the cytoplasm that lacked ER (**Figure 7E,G**). Deletion of the repeat regions in GFP::ANC-1b:: Δ 6RPS led to a re-localization away from the general ER (**Figure 7F–G**). Together, these results suggest that (1) ANC-1b has a similar distribution pattern as the ER and (2) that the transmembrane span and repeat regions, but not the luminal KASH domain, plays roles ANC-1 ER localization. The ANC-1 localization pattern is consistent with the above findings that *anc-1*(Δ 6RPS) *anc-1*(Δ TK) mutants had intermediate nuclear and ER positioning defects, worse than *anc-1*(Δ 25KASH) mutants.

Other organelles are mis-localized in *anc-1* mutants

Our imaging showed that both nuclei and the ER are both unanchored and move freely throughout the cytoplasm. Furthermore, our deletion analyses cast significant doubt on the old tethering model. In our new model, without ANC-1, the entire cytoplasm is disconnected and multiple organelles are likely flowing freely throughout the cytoplasm. We therefore used the MDT-28::mCherry (Na *et al.*, 2015) marker to follow lipid droplets (**Figure 8, Videos 4–5**) and the mitoLS::GFP marker to follow mitochondria (**Figure 9, Videos 6–7**). In *anc-1* null mutant animals, both lipid droplets and

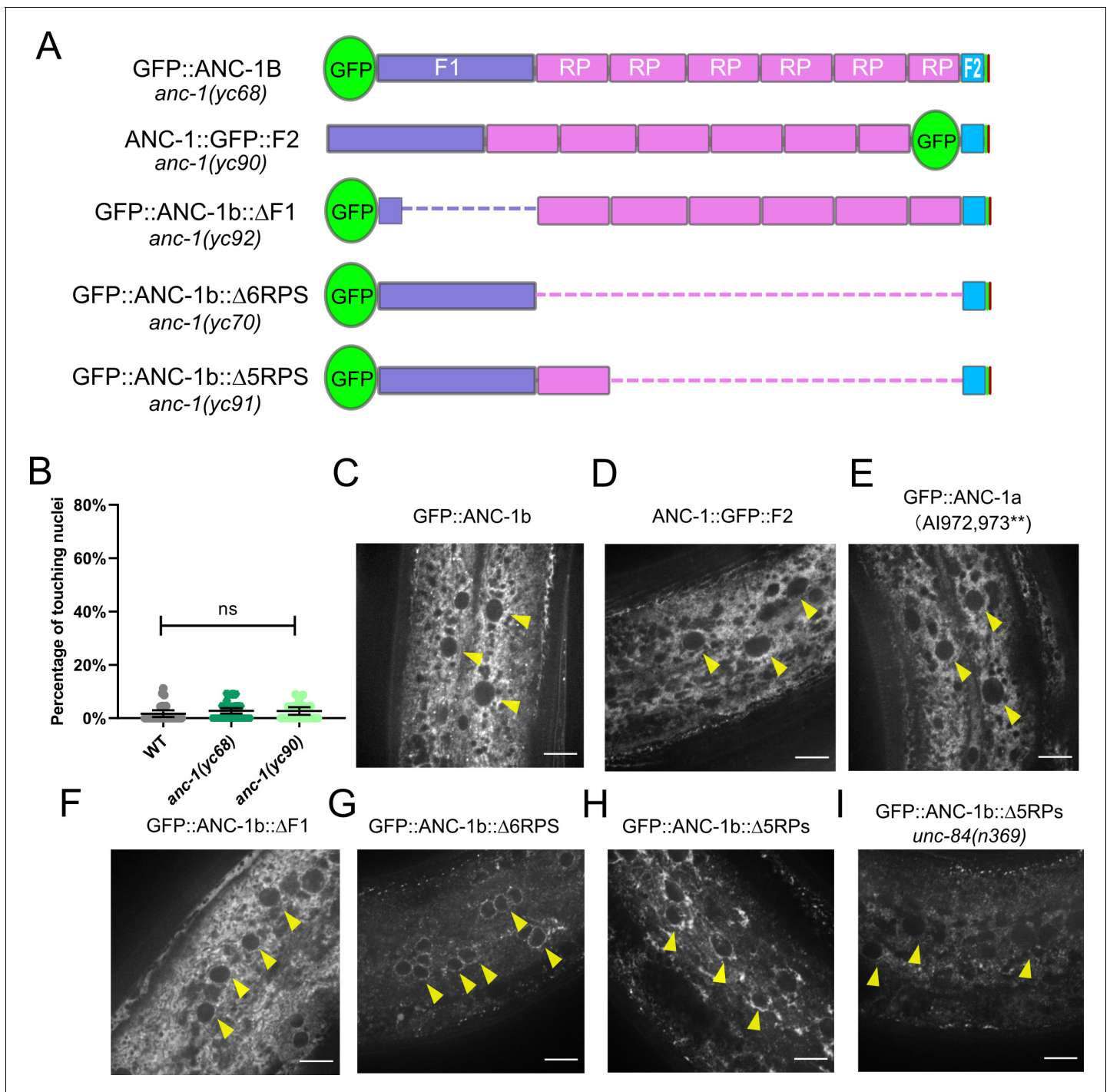


Figure 5. The subcellular localization of ANC-1. (A) Schematic depicting the ANC-1 GFP knock-in constructs with or without deletion of ANC-1 cytoplasmic domains. (B) Nuclear positioning in GFP::ANC-1b is wild type (WT). Each point represents the percentage of touching nuclei on one side of a young adult animal. Means with 95% CI error bars are shown. ns, not significant ($p > 0.05$). $n \geq 20$. (C–I) Confocal images of hyp7 subcellular localization in the indicated strains. Yellow arrowheads point to nuclei. Scale bar, 10 μm .

The online version of this article includes the following figure supplement(s) for figure 5:

Figure supplement 1. GFP::ANC-1($\Delta 6\text{RPS}$) is expressed at a lower level and is enriched at the nuclear envelope.

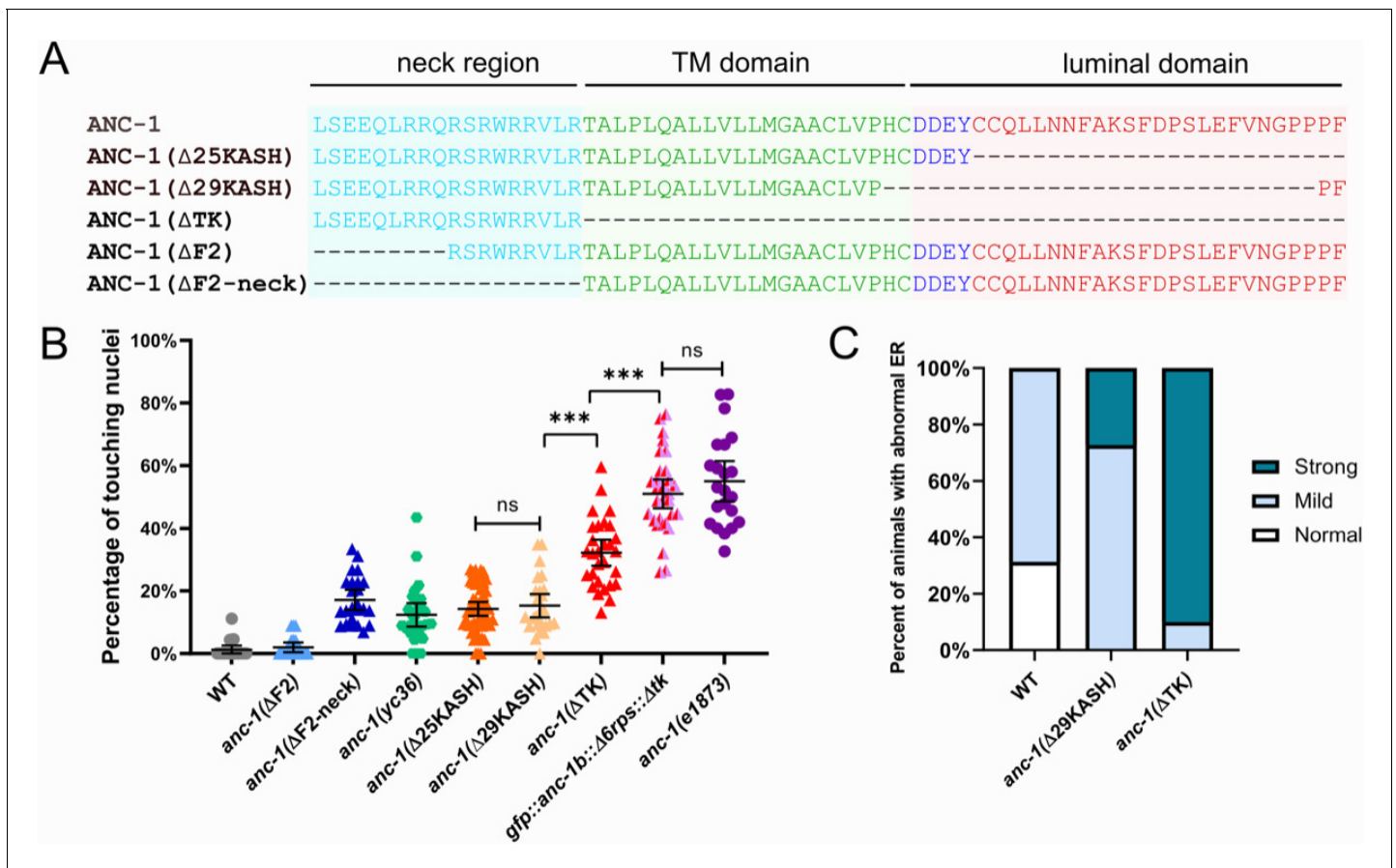


Figure 6. The transmembrane domain of ANC-1 is necessary for nuclear and ER positioning. (A) Sequence of deletion in the neck region (blue), transmembrane (TM) span (green), or the luminal domain (red). (B) Quantification of nuclear anchorage defects in *anc-1* mutants. Each point represents the percentage of touching nuclei on one side of a young adult animal. Means with 95% CI error bars are shown. $n \geq 20$. ANOVA and Tukey's multiple comparisons tests were used in comparisons. *** $p \leq 0.001$; ns means $p > 0.05$. The data of wild type (WT), *anc-1*(Δ F2), *anc-1*(Δ 25KASH), *anc-1*(Δ 29KASH), and *anc-1*(e1873) are duplicated from **Figures 1C** and **3C** and copied here for easy reference. (C) Qualitative analysis of the ER anchorage defects as in **Figure 4**. Significantly more *anc-1*(Δ TK) animals show strong ER anchorage defects than *anc-1*(Δ 29KASH) mutants ($p \leq 0.01$ by Fisher's exact test). Sample sizes were all ≥ 10 .

mitochondria moved in a manner suggesting they were not connected to a network. Furthermore, lipid droplets were often seen in large clusters and mitochondria appeared slightly fragmented. We therefore conclude that ANC-1 is required to interconnect the entire cytoplasm to anchor nuclei, ER, lipid droplets, mitochondria, and likely other organelles to a single network that regulates the integrity of the cytoplasm.

Microtubule networks appear normal in *anc-1* mutants

One hypothesis for ANC-1 function is that it regulates cytoskeletal networks. In this model, mutations in *anc-1* would disrupt the cytoskeleton, causing organelles to lose their attachment to the cytoskeleton and move around freely as shown in **Figures 4, 8** and **9**. We therefore examined microtubule organization in the hyp7 syncytia of wild type and *anc-1* null mutant animals. We followed microtubules in live animals with an endogenously expressed microtubule binding protein, GFP::MAPH-1.1 (**Castiglioni et al., 2020; Waaijers et al., 2016**). The density and relative disorganization of the microtubule network in wild type made it difficult to quantify any growth, length, or number parameters of microtubules. Nonetheless, qualitatively, in comparison with the wild type (**Video 8**), microtubules were mostly normal in *anc-1* null mutant animals (**Figure 10** and **Videos 9–10**). The exception was where nuclei had moved back and forth along an anterior-posterior axis, they appear to have cleared a microtubule free channel. These results are more in line with a model where in the

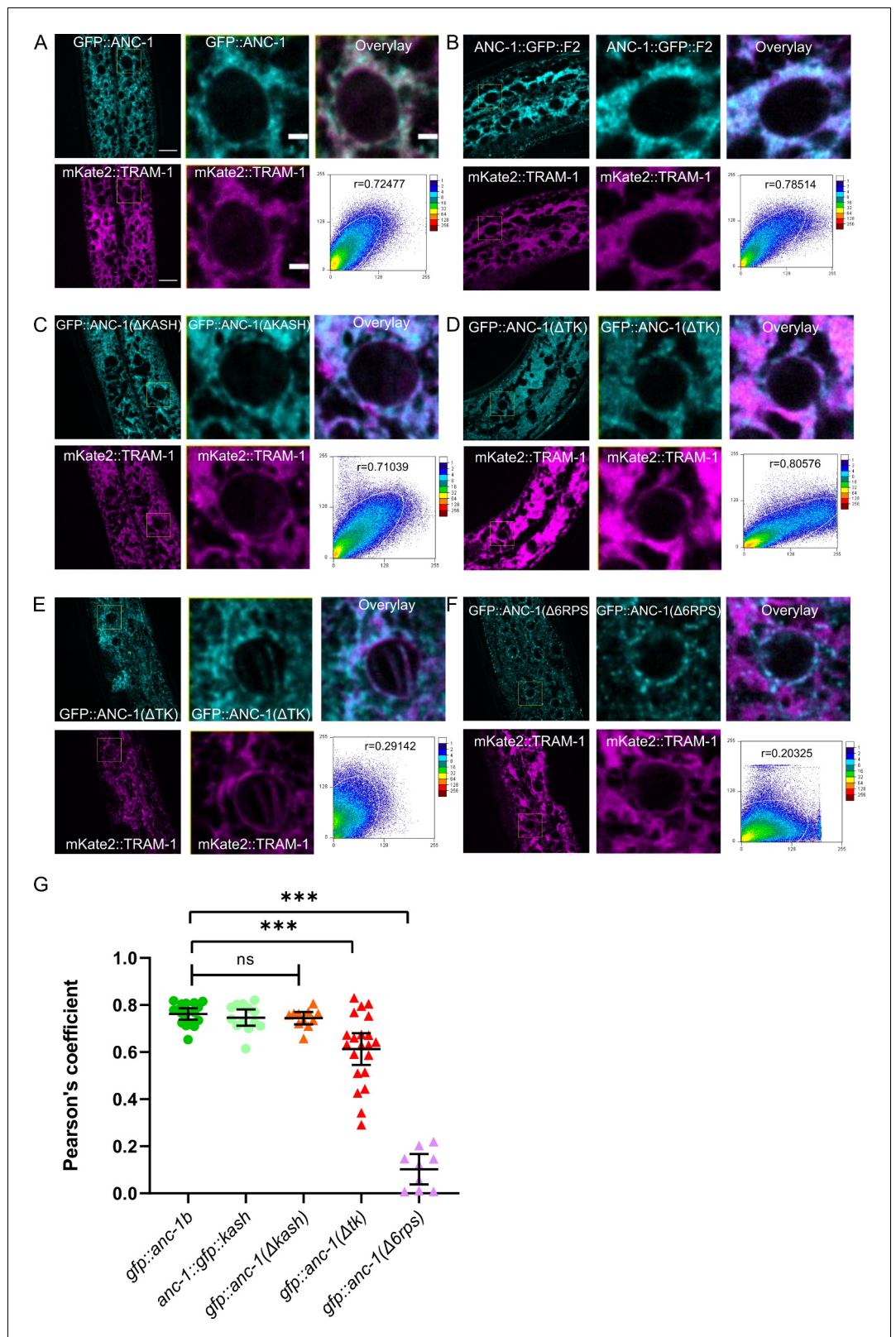


Figure 7. ANC-1 localizes to the ER. ANC-1-GFP fusion protein (cyan) localization with respect to the ER membrane as marked by a mKate2::TRAM-1 (magenta) is shown. (A) Wild type (WT) GFP::ANC-1b. (B) Wild type ANC-1::GFP::F2. (C) GFP::ANC-1b:: Δ KASH. (D) An example of GFP::ANC-1b:: Δ TK with good overlap with the ER and (E) a GFP::ANC-1b:: Δ TK with poor overlap. (F) GFP::ANC-1b:: Δ 6RPS. (A–F) For each section, the left two *Figure 7 continued on next page*

Figure 7 continued

panels are low magnification of the young adult hypodermis (scale bar, 10 μm) and the middle two panels are a zoom in of the boxed part of the left panels (scale bar, 2 μm). The top right shows the merge of the two channels. The bottom right uses the used ImageJ plug-in ScatterJ to quantify the co-localization and the Pearson's correlation coefficient for overlap is shown as an r value. (G) A scatter plot of Pearson's coefficients showing overlap between the indicated GFP and the mKate::TRAM-1 ER membrane marker. Mean \pm 95% CI are shown. ANOVA and Tukey's multiple comparisons tests were used in comparisons. *** $p \leq 0.001$; ns means not significant. The online version of this article includes the following figure supplement(s) for figure 7:

Figure supplement 1. GFP::ANC-1b does not co-localize with lipid droplets or mitochondria.

absence of ANC-1, nuclei move around and disrupt or move microtubules in their way rather than a model where a lack of ANC-1 leads to massive microtubule disruption that then frees nuclei and other organelles to move throughout the syncytia.

Depletion of ANC-1 disrupts nuclear morphology and causes developmental defects

Nuclear shape changes were observed during live imaging in *anc-1* mutants consistent with a model where *anc-1* mutant nuclei are susceptible to pressures from the cytoplasm, perhaps crashing into other organelles that corresponded with dents in nuclei. We therefore quantified nuclear size and

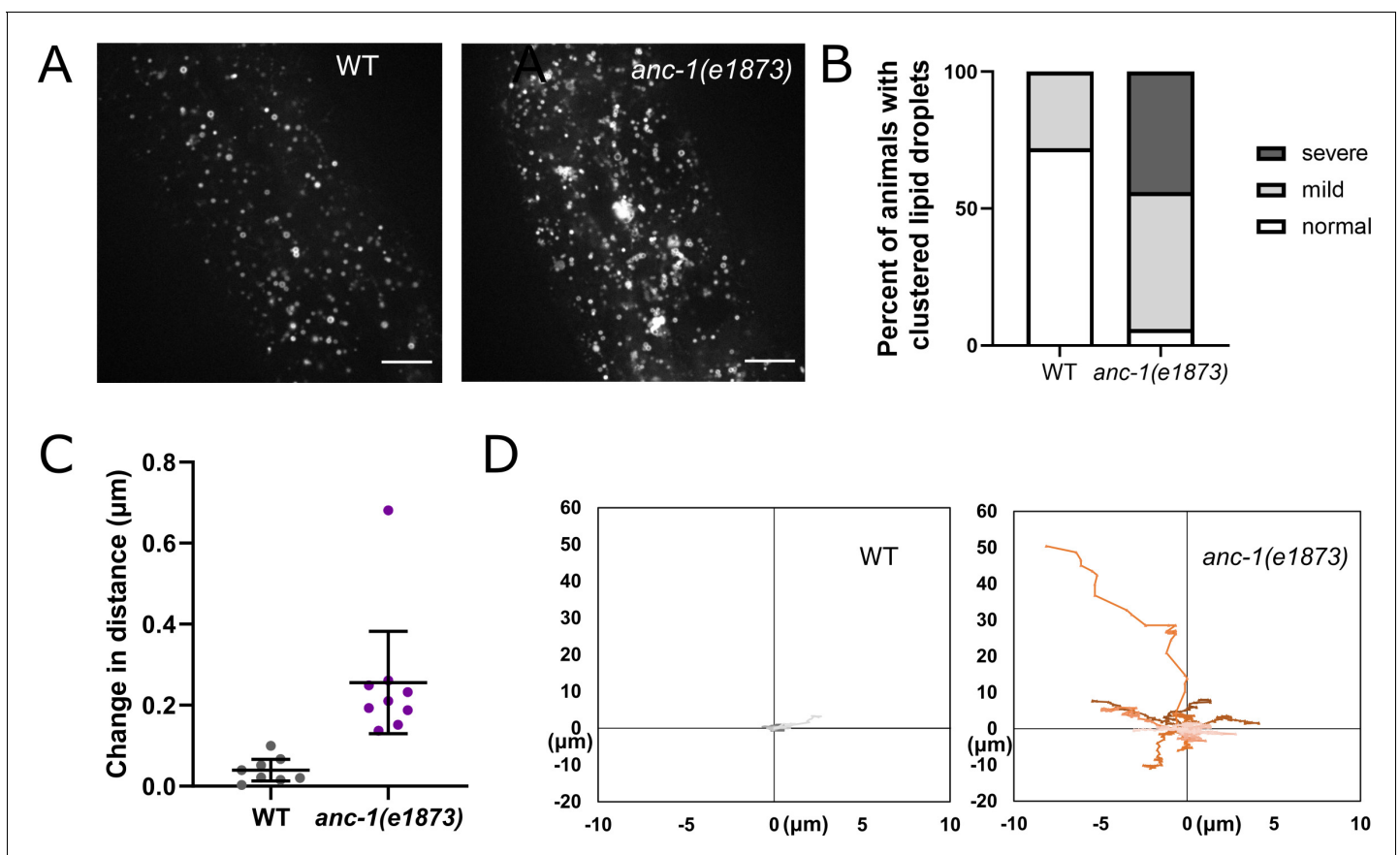
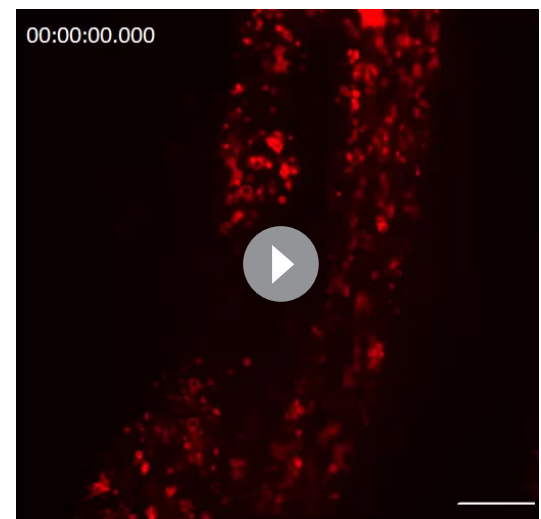


Figure 8. Lipid droplets are mispositioned in *anc-1* mutants. (A) Representative images of hyp7 lipid droplets labeled with the $P_{mdt-28}::mdt-28::mCherry$ marker in the young adult animals. (B) Scoring of the lipid droplet positioning defects. Images were randomized for blind analysis by multiple researchers. $n \geq 11$. (C–D) Time-lapse images of hyp7 lipid droplets. (C–D) The lipid droplet displacement phenotype was quantified as described in Figure 4E–F. The average change in distance between two points in 242 ms intervals is plotted in (C). The trajectories of the relative movements of each spot apart from the others are shown in (D). Eight movies of each strain were analyzed. Scale bar, 10 μm for all the images. Also see Videos 4–5. WT = wild type.



Video 4. Lipid droplets are anchored in wild type (WT) hyp7. An example video of the hyp7 lipid droplets in young adult wild type *C. elegans* expressing *ldr1s2* [*mdt-28p::mdt-28::mCherry +unc-76(+)*]. Images were captured at the interval of 0.2 s for 10 s. Scale bar, 10 μ m.

<https://elifesciences.org/articles/61069#video4>



Video 5. Lipid droplets are unanchored in *anc-1(e1873)* mutant hyp7. An example video of the hyp7 lipid droplets in the young adult *anc-1(e1873)* mutant *C. elegans* expressing *ldr1s2* [*mdt-28p::mdt-28::mCherry +unc-76(+)*]. Images were captured at the interval of 0.24 s for 10 s. Scale bar, 10 μ m.

<https://elifesciences.org/articles/61069#video5>

shape in *anc-1* mutants to better characterize how nuclear and/or ER movements affect the nuclear structure. Adult syncytial hyp7 nuclei were significantly smaller in *anc-1(Δ 6RPS)* and *anc-1(e1873)* mutants compared to wild type (**Figure 11A**). Furthermore, the shape of *anc-1(e1873)* hyp7 nuclei, as measured by circularity and solidity, was significantly less round than wild type (**Figure 11B**).

Given the nuclear anchorage, ER positioning, and nuclear shape defects observed in *anc-1* mutants, we examined whether these animals might have other developmental or growth defects. Despite producing fertile adults, *anc-1* null animals had severe developmental defects. The brood size of *anc-1(e1873)* mutants was less than 25% of wild type (**Figure 11C**) and *anc-1(e1873)* mutants had significantly smaller body sizes throughout larval and adult stages (**Figure 11D–F**). Together these results suggest that there are developmental consequences associated with organelle positioning defects in *anc-1* mutants.

Discussion

LINC complexes consisting of giant KASH proteins (*C. elegans* ANC-1, *Drosophila* MSP300, and mammalian Nesprin-1 and -2) and canonical SUN proteins (*C. elegans* UNC-84, *Drosophila* Koi, and mammalian Sun1 and Sun2) are thought to anchor nuclei by tethering them to the cytoskeleton (**Starr and Fridolfsson, 2010**). ANC-1 was thought to connect actin filaments to the nuclear envelope using conserved CH and KASH domains at its N- and C-termini, respectively (**Starr and Han, 2002**). However, results discussed below indicate that this model is not sufficient to explain the role of KASH proteins in the cell. We propose a cytoplasmic integrity model, where giant KASH proteins function, largely independently of LINC complexes at the nuclear envelope and through mechanisms that do not require their CH domains. We find ANC-1 also localizes close to the ER throughout the cell. The large cytoplasmic domains of ANC-1 are required for positioning nuclei, ER, and likely other organelles. In the absence of ANC-1, the contents of the cytoplasm are disconnected from each other, unanchored in place, and sometimes fragmented. The cytoplasm and organelles freely flow throughout the hypodermal syncytia as worms crawl. It appears that ANC-1 is required to organize the entire cytoplasm.

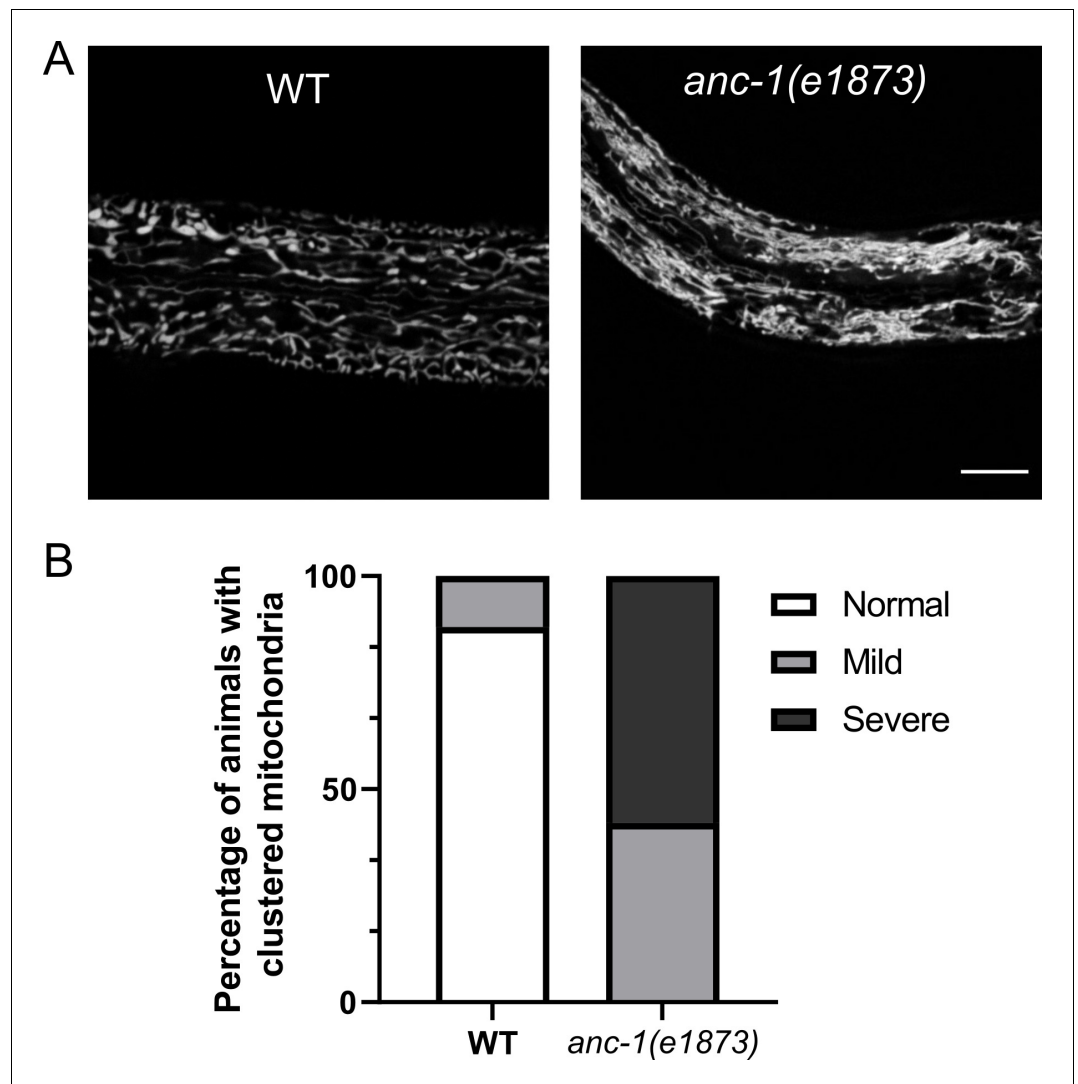
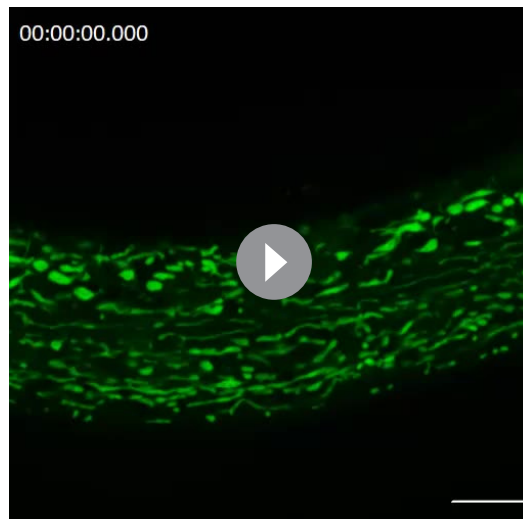


Figure 9. Mitochondria are mispositioned in *anc-1* mutants. (A) The *hyp7* mitochondria were labeled with the $P_{col-10}::mito::GFP$ marker in the L3 animals. (B) The mitochondria positioning defect was scored. Images were randomized for blind analysis by multiple researchers. $n \geq 18$ for each strain. Scale bar, 10 μm for all the images. Also see **Videos 6–7**. WT = wild type.

Our finding that ANC-1 works independently of LINC complexes during *hyp7* nuclear positioning has significant implications for how the field currently understands the role of LINC complexes in development and disease. A dominant negative approach relies on overexpression of KASH domains to displace endogenous KASH proteins from the nuclear envelope (Grady et al., 2005; Starr and Han, 2002; Tsujikawa et al., 2007). Alternatively, a mini-nesprin-2 construct, consisting of the calponin homology and KASH domains with a few spectrin repeats, is commonly used in rescue experiments (Davidson et al., 2020; Luxton et al., 2010; Ostlund et al., 2009). If ANC-1 and other giant KASH orthologs have major LINC complex-independent functions, these approaches might have more caveats than previously thought.

We found that the CH domain of ANC-1 is dispensable for ER and nuclear positioning. Similar findings suggest the Nesprin-1 or -2 CH domains are also dispensable for the development of mouse skeletal muscles and the epidermis (Lüke et al., 2008; Stroud et al., 2017). Moreover, the CH domains are not required for Nesprin-2 mediated neuronal migration in the developing rat brain (Gonçalves et al., 2020). Thus, the significance of the conserved CH domain is not clear. The CH domain of Nesprin-2 is required to form transmembrane actin-associated lines on the nuclear



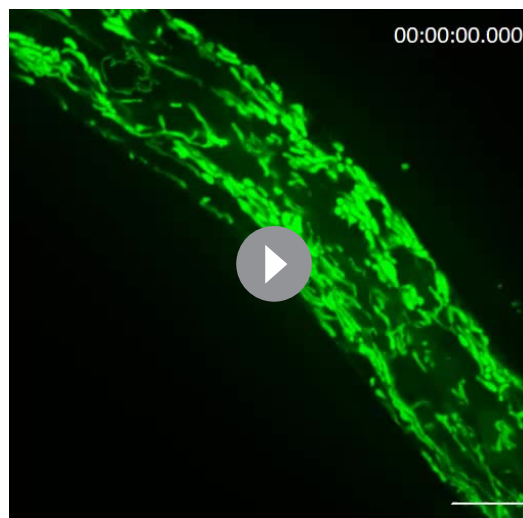
Video 6. Mitochondria are anchored in wild type (WT) hyp7. An example video of hyp7 mitochondria in young adult wild type *C. elegans* as followed by the $P_{col-10}::mitoLS::GFP$ marker. Images were captured at the interval of 0.1 s for 10 s. Scale bar, 10 μ m. <https://elifesciences.org/articles/61069#video6>

mostly localize away from nuclei and are only clearly enriched at the nuclear periphery in the somatic gonad (Starr and Han, 2002) and Nesprin-1 localizes to ciliary rootlets (Potter et al., 2017). Yet, most models, including the nuclear tethering model, focus primarily on nuclear envelope localization. We found that GFP::ANC-1b was not enriched at the nuclear envelope in most tissues (Figure 5—

envelope during rearward nuclear movement in mouse NIH3T3 fibroblasts polarizing for migration and to accumulate Nesprin-2 at the front of nuclei in cultured mouse embryonic fibroblasts migrating through constrictions (Davidson et al., 2020; Luxton et al., 2010).

Most of the other ANC-1 domains, including the C-terminal transmembrane span and the large cytoplasmic repeat regions, are required for nuclear anchorage. Portions of the tandem repeats may be arranged in bundles of three helices, reminiscent of spectrin repeats (Liem, 2016). Thus, we hypothesize that ANC-1, like the other giant KASH orthologs MSP300 and Nesprin-1 and -2, consists largely of spectrin repeats with a C-terminal transmembrane domain that attaches ANC-1 to the contiguous ER and outer nuclear membrane.

In general, giant KASH proteins localize strongly to the nuclear envelope in multiple systems (Starr and Fridolfsson, 2010). Evidence for giant KASH protein localization to other subcellular locations has been largely ignored or attributed to overexpression artifacts (Zhang et al., 2001) or the loss of KASH protein function (Roux et al., 2009). Antibodies against ANC-1



Video 7. Mitochondria are unanchored in *anc-1(e1873)* mutant hyp7. An example video of hyp7 mitochondria in the young adult *anc-1(e1873)* mutant *C. elegans* as followed by the $P_{col-10}::mitoLS::GFP$ marker. Images were captured at the interval of 0.1 s for 10 s. Scale bar, 10 μ m. <https://elifesciences.org/articles/61069#video7>



Video 8. Microtubules in wild type (WT) hypodermal syncytia. A representative clip of the hyp7 in a wild type young adult expressing GFP::MAPH-1.1 to mark microtubules in cyan and EMR-1::mCherry to mark nuclear envelopes in magenta. Images were at the interval of 1 s for 20 s. Scale bar, 10 μ m. <https://elifesciences.org/articles/61069#video8>

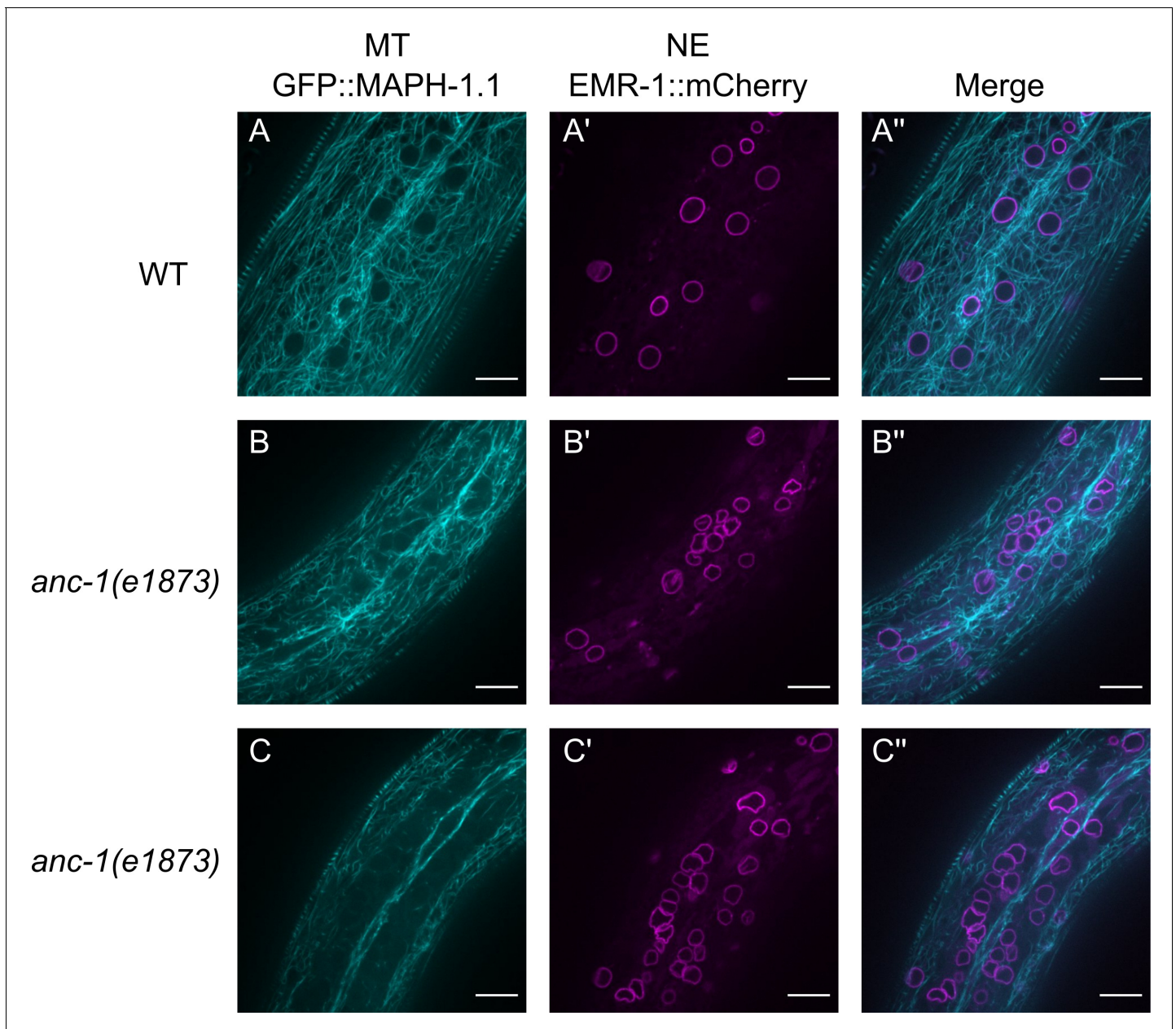
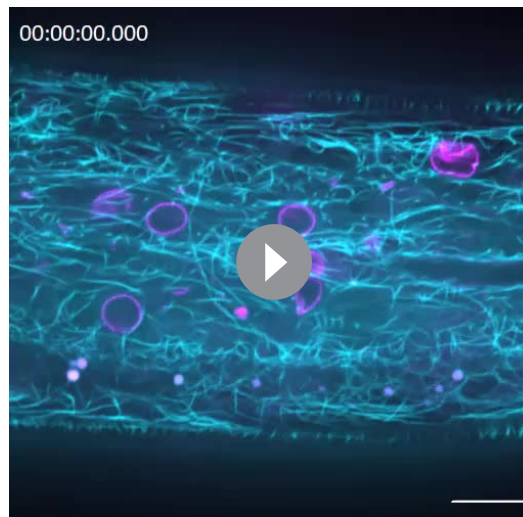


Figure 10. Microtubule organization in *anc-1* mutants. Representative images of microtubules (cyan) and nuclear envelope (NE) (magenta) from the same young adult animals are shown. (A–A'') wild type (WT), (B–B'') *anc-1(e1873)* mutant animal where the microtubules are mostly normal. (C–C'') In other *anc-1(e1873)* animals, microtubule organization is disrupted in the channels where nuclei move. Microtubules are labeled with GFP::MAPH-1.1 and the nuclear envelope is labeled with EMR-1::mCherry. Scale bar, 10 μ m. Also see **Videos 8–10**.

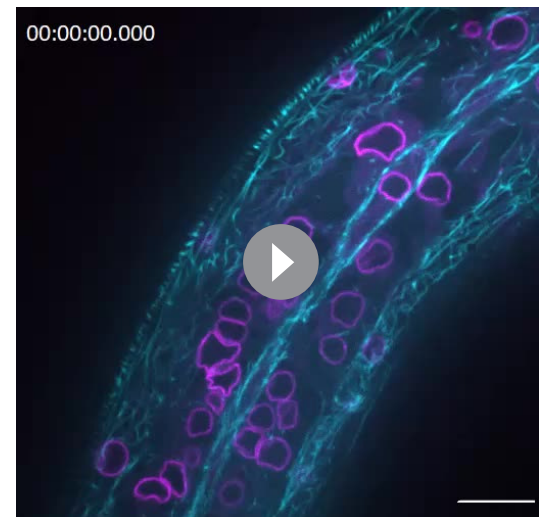
figure supplement 1). Instead, our findings suggest that ANC-1 functions throughout the cytoplasm with its C-terminus in the ER membrane.

We observed that the ER is severely mispositioned in *anc-1* null mutant hypodermal cells. Also, mitochondria are misshaped and mispositioned in the *anc-1* null mutants, but not in *unc-84* nulls (Hedgecock and Thomson, 1982; Starr and Han, 2002). Two different mechanisms could explain how nuclei, mitochondria, and the ER are all mispositioned in *anc-1* mutants. First, abnormal organelle clusters could result from a failure in the active positioning process (Folker and Baylies, 2013; Roman and Gomes, 2018). Alternatively, organelles could lose physical connections to the rest of the cytoplasm, resulting in organelles being passively pushed around in response to external mechanical forces, such as those generated when the worm crawls. Live imaging favors the second



Video 9. Microtubules in *anc-1(null)* hypodermal syncytia. A representative clip of the hyp7 in a *anc-1* (*e1783*) mutant young adult expressing GFP::MAPH-1.1 to mark microtubules in cyan and EMR-1::mCherry to mark nuclear envelopes in magenta. Images were at the interval of 0.845 s for 40 s. Scale bar, 10 μ m.

<https://elifesciences.org/articles/61069#video9>



Video 10. Microtubules in *anc-1(null)* hypodermal syncytia. A representative clip of the hyp7 in a *anc-1* (*e1783*) mutant young adult expressing GFP::MAPH-1.1 to mark microtubules in cyan and EMR-1::mCherry to mark nuclear envelopes in magenta. Images were at the interval of 0.638 s for 32 s. Scale bar, 10 μ m.

<https://elifesciences.org/articles/61069#video10>

model. As *anc-1* mutant worms bent their bodies, ER fragments rapidly moved in a bulk flow of cytoplasm along with nuclei. The nuclei became misshapen and the ER often fragmented. Nuclei and the ER appeared to be completely detached from any sort of cytoplasmic structural network in *anc-1* mutants. There is precedent that giant KASH proteins could mechanically stabilize the cytoplasm. In cultured mouse NIH3T3 fibroblasts, disrupting KASH proteins leads to the decreased stiffness across the entire cell, as determined by single-particle microrheology experiments (Stewart-Hutchinson *et al.*, 2008). Therefore, we propose that ANC-1 and other giant KASH proteins normally function at the ER periphery as important crosslinkers to maintain the mechanical integrity of the cell.

ANC-1 likely maintains the mechanical integrity of the cytoplasm via cytoskeletal networks. Disruption of MSP300 leads to disruption of both actin and microtubule networks in *Drosophila* muscles (Wang *et al.*, 2015). Giant KASH proteins can interact with actin independently of their CH domains. ANC-1 binds to AMPH-1/BIN1, which is involved in actin nucleation (D'Alessandro *et al.*, 2015), and Nesprin-2 binds to the actin regulators Fascin and FHOD1 (Jayo *et al.*, 2016; Kutscheidt *et al.*, 2014). Nesprin-1 interacts with Akap450 to form microtubule organizing centers at the nuclear envelope of mouse muscles (Elhanany-Tamir *et al.*, 2012; Gimpel *et al.*, 2017; Zheng *et al.*, 2020). Intermediate filaments and spectraplakins have also been implicated in nuclear positioning (Ralston *et al.*, 2006; Wang *et al.*, 2015; Zheng *et al.*, 2020). However, *anc-1* null mutant animals had a reasonably normal microtubule network. Thus, how ANC-1b might directly interact with cytoskeletal components requires further investigations.

In summary, we propose a cytoplasmic integrity model, for how ANC-1 and giant KASH orthologs position nuclei and other organelles. First, ANC-1 is targeted to the ER through its C-terminal transmembrane span. The large cytoplasmic domain of ANC-1 likely consists of divergent spectrin-like repeats that could serve as elastic filaments. ANC-1 filaments could interact with various components of the cytoskeleton, allowing ANC-1 to serve as a cytoskeletal crosslinker to maintain the mechanical integrity of the cytoplasm. However, since at least microtubules are not completely disrupted, ANC-1 likely functions to maintain the mechanical properties of the cytoplasm through other mechanisms. Extracellular mechanical pressure that is generated as the worm bends leads to rapid cytoplasmic fluid flows and positioning defects in nuclei, ER, mitochondria, and likely other

organelles. In this model, ANC-1 maintains cellular connectivity across the cytoplasm by anchoring organelles in place.

Materials and methods

Key resources table

Reagent type (species) or resource	Designation	Source or reference	Identifiers	Additional information
Strain, strain background (<i>Escherichia. coli</i>)	OP50	Caenorhabditis Genetics Center (CGC)	OP50	https://cgc.umn.edu/strain/OP50
Strain, strain background (<i>E. coli</i>)	DH10B	New England Biolabs (NEB)	C3019H	
Recombinant DNA reagent	pLF3FShC	Nonet, 2020	addgene: #153083	https://www.addgene.org/153083/
Recombinant DNA reagent	pSL845	This paper		<i>P_{y37a1b.5::mKate2::tram-1::tram-1}</i> 3'UTR plasmid to generate the <i>ycSi2</i> transgenic <i>C. elegans</i> strain
Recombinant DNA reagent	pSL835	This paper		<i>P_{anc-1b::nls::gfp::lacZ}</i> Plasmid to generate <i>ycEx260</i>
Recombinant DNA reagent	pSL289	This paper		<i>P_{col-10::mitoLS::gfp}</i> Plasmid to generate <i>ycEx217</i>

C. elegans genetics

C. elegans strains were maintained on nematode growth medium plates seeded with OP50 *E. coli* at the room temperature (approximately 22°C) (Brenner, 1974). All the strains used in this study are listed in **Table 1**. Some strains, including N2 (WB Cat# WBStrain00000001, RRID:WB-STRAIN:WBStrain00000001), which was used as wild type, were obtained from the Caenorhabditis Genetics Center, funded by the National Institutes of Health Office of Research Infrastructure Programs (P40 OD010440). Strains VC40007, VC20178, and VC40614 were provided by the *C. elegans* Reverse Genetics Core Facility at the University of British Columbia (Thompson et al., 2013). Strain RT3739 (*pwSi83*) was generously provided by Barth Grant (Rutgers University, NJ, USA). UD522 (*ycEx249* [*pcol-19::gfp::lacZ*, *pmyo-2::mCherry*]) was previously described (Cain et al., 2018). Male strains of RT3739, UD522, BOX188, LIU2, UD756, UD3, and BN147 were made to cross into *anc-1* or *unc-84* mutants. Alternatively, *pcol-19::gfp::lacZ* was introduced into some mutants by standard germline transformation to make UD736 and UD737 (Cain et al., 2018; Mello et al., 1991).

For *anc-1* RNAi feeding experiments, L4 stage animals were transferred onto NGM plates seeded with bacteria expressing dsRNA (Timmons and Fire, 1998). The clones from the Ahringer RNAi library (Source Bioscience) (Kamath and Ahringer, 2003) were confirmed by Sanger sequencing.

Nuclear anchorage assays were performed as described (Cain et al., 2018; Fridolfsson et al., 2018). Briefly, L4 worms with GFP-marked hypodermal nuclei were picked onto fresh plates 20 hr before scoring. Young adults were mounted on 2% agarose pads in ~5 µl of 1 mM tetramisole in M9 buffer (Fridolfsson et al., 2018). Syncytial hyp7 nuclei were scored as touching if a nucleus was in contact with one or more neighboring nuclei. Only one lateral side of each animal was scored.

For the brood size assay, starting at the L4 stage, single animals were transferred onto fresh OP50 *E. coli* plates every 24 hr for seven days. The number of embryos laid were counted immediately after the removal of the animal each day.

To measure body size, embryos laid within an hour were collected and cultured for 24 hr and 69 hr to reach the L2 stage and the adult stage, respectively. Animals were mounted on 2% agarose pads in ~5 µl of 1 mM tetramisole in M9 buffer for imaging.

5'-Rapid amplification of cDNA ends (5'-RACE)

Total RNA was extracted from mixed stages of *C. elegans* using the RNeasy kit (QIAGEN). First-strand cDNAs were generated with the ThermoScript RT-PCR system using an *anc-1* antisense

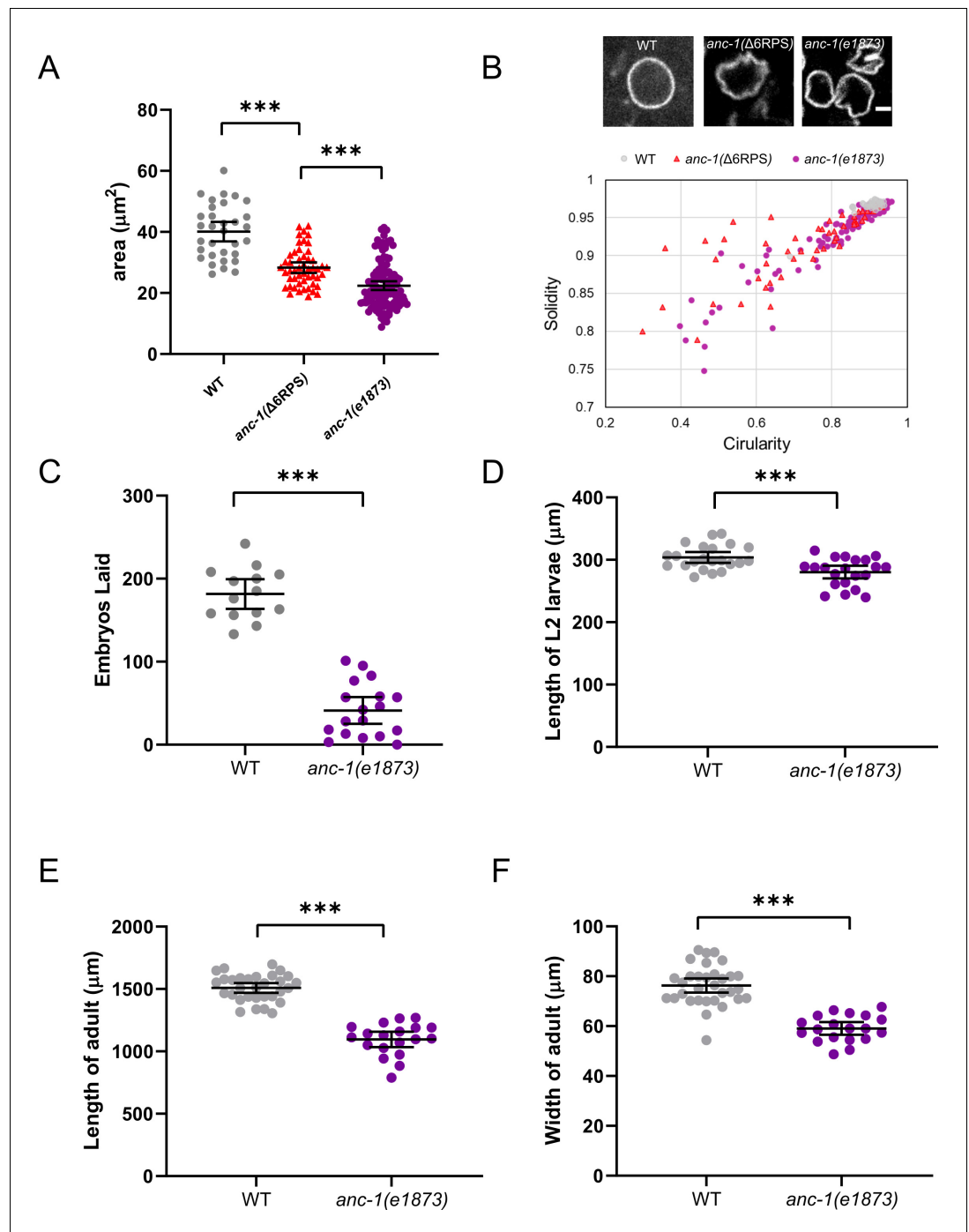


Figure 11. *anc-1* mutants have developmental defects. (A) The area of cross-sections of hyp7 nuclei is shown. Each dot represents the area of a single nucleus. $n = 32$ for wild type (WT), $n = 50$ for *anc-1*($\Delta 6RPS$), $n = 111$ for *anc-1*(*e1873*). (B) Top panel: Representative images of hyp7 nuclei marked by EMR-1::mCherry of WT, *anc-1*($\Delta 6RPS$), and *anc-1*(*e1873*) mutants. Scale bar, 2 μm . Bottom panel: Plot of the solidity and the circularity. (C–F) The brood size (C), length of the L2 larvae (D), adult length (E) and width (F) are significantly reduced in *anc-1*(*e1873*) mutants. Each dot represents a single animal. $n \geq 14$ for (C) and $n \geq 19$ for (D–F). Means with 95% CI error bars are shown. Unpaired student two-tail t-test was used for statistical analysis. ** $p \leq 0.01$; *** $p \leq 0.001$.

oligonucleotide (ods2572: 5'-ATAGATCATTACAAGATG-3'). Purification and TdT tailing of the first-strand cDNA were performed by the 5' RACE System for Rapid Amplification of cDNA Ends, version 2.0 (Invitrogen, Cat. No. 18374058). The target cDNA was amplified PCR using the provided 5'

Table 1. *C. elegans* strains in this study.

Strain	Genotype	Reference
N2	Wild type	
UD522	<i>ycEx249</i> [<i>p_{col-19}::gfp::lacZ</i> , <i>p_{myo-2}::mCherry</i>]	Cain et al., 2018
UD532	<i>unc-84(n369) X</i> ; <i>ycEx249</i>	Cain et al., 2018
UD538	<i>anc-1(e1873) I</i> ; <i>ycEx249</i>	Cain et al., 2018
UD578	<i>anc-1(yc52[Δ25KASH]) I</i> ; <i>ycEx249</i>	This study
UD615	<i>anc-1(yc69[Δ29KASH]) I</i> ; <i>ycEx249</i>	This study
JR672	<i>wls54[scm::gfp] V</i>	Terns et al., 1997
UD457	<i>unc-84(n369) X</i> ; <i>wls54 V</i>	This study
UD451	<i>anc-1(e1873) I</i> ; <i>wls54 V</i>	This study
VC20178	<i>anc-1(gk109010[W427*]) I</i>	Thompson et al., 2013
UD737	<i>anc-1(gk109010[W427*]) I</i> ; <i>ycEx265</i> [<i>p_{col-19}::gfp::lacZ</i> , <i>p_{myo-2}::mCherry</i>]	This study
VC40007	<i>anc-1(gk109018[W621*]) I</i>	Thompson et al., 2013
UD736	<i>anc-1(gk109018[W621*]) I</i> ; <i>ycEx266</i> [<i>p_{col-19}::gfp::lacZ</i> , <i>p_{myo-2}::mCherry</i>]	This study
VC40614	<i>anc-1(gk722608[Q2878*]) I</i>	Thompson et al., 2013
UD565	<i>anc-1(gk722608[Q2878*]) I</i> ; <i>ycEx249</i>	This study
UD535	<i>anc-1(yc41[anc-1::gfp3Xflag::kash,Δch]) I</i> ; <i>ycEx249</i>	This study
UD608	<i>ycEx260</i> [<i>p_{anc-1b}::nls::gfp::lacZ</i>]	This study
UD599	<i>anc-1(yc62[ΔF1]) I</i> ; <i>ycEx249</i>	This study
UD591	<i>anc-1(yc61[Δ6RPS]) I</i> ; <i>ycEx249</i>	This study
UD668	<i>anc-1(yc80[ΔF2]) I</i> ; <i>ycEx249</i>	This study
UD669	<i>anc-1(yc81[ΔF2-neck]) I</i> ; <i>ycEx249</i>	This study
UD695	<i>anc-1(yc61[Δ6RPS]) I</i> ; <i>unc-84(n369) X</i> ; <i>ycEx249</i>	This study
UD696	<i>anc-1(yc62[ΔF1]) I</i> ; <i>unc-84(n369) X</i> ; <i>ycEx249</i>	This study
UD612	<i>anc-1(yc68[gfp::anc-1b]) I</i>	This study
UD655	<i>anc-1(yc78[Δ5RPS]) I</i> ; <i>ycEx249</i>	This study
UD619	<i>anc-1(yc68[gfp::anc-1b]) I</i> ; <i>ycEx249</i>	This study
UD694	<i>anc-1(yc90[anc-1::gfp::F2]) I</i>	This study
UD697	<i>anc-1(yc90[anc-1::gfp::F2]) I</i> ; <i>ycEx249</i>	This study
UD618	<i>anc-1(yc70[gfp::anc-1b::Δ6rps]) I</i>	This study
UD698	<i>anc-1(yc91[gfp::anc-1b::Δ5rps]) I</i>	This study
UD701	<i>anc-1(yc92[gfp::anc-1b::Δf1]) I</i>	This study
UD702	<i>anc-1(yc93[anc-1A1972,973**::gfp]) I</i>	This study
UD625	<i>anc-1(yc71[ΔTK]) I</i> ; <i>ycEx249</i>	This study
UD645	<i>anc-1(yc73[gfp::anc-1b::Δ6rps::Δtk]) I</i> ; <i>ycEx249</i>	This study
RT3739	<i>pwSi83</i> [<i>p_{hyp7}gfp::kdel</i>]	A gift from Barth Grant
UD652	<i>anc-1(e1873) I</i> ; <i>pwSi83</i>	This study
UD679	<i>unc-84(n369) X</i> ; <i>pwSi83</i>	This study
UD707	<i>anc-1(yc71[ΔTK]) I</i> ; <i>pwSi83</i>	This study
UD651	<i>anc-1(yc61[Δ6RPS]) I</i> ; <i>pwSi83</i>	This study
UD672	<i>anc-1(yc69[Δ29KASH]) I</i> ; <i>pwSi83</i>	This study
UD520	<i>anc-1(yc36[anc-1::gfp3Xflag::kash]) I</i>	This study

Table 1 continued on next page

Table 1 continued

Strain	Genotype	Reference
BN147	bqSi142 [<i>p_{emr-1}::emr-1::mCherry + unc-119(+)</i>] II	Morales-Martínez et al., 2015
BOX188	<i>maph-1.1(mib12[gfp::maph-1.1]) I</i>	Waaijers et al., 2016
UD649	<i>maph-1.1(mib12[gfp::maph-1.1]) I; bqSi142 II</i>	This study
UD650	<i>anc-1(e1873) I; maph-1.1(mib12[gfp::maph-1.1]) I; bqSi142 II</i>	This study
UD677	<i>anc-1(yc61[Δ6RPS]) I; maph-1.1(mib12[gfp::maph-1.1]) I; bqSi142 II</i>	This study
UD3	<i>ycEx217[P_{col-10}::mitoLS::GFP, P_{odr-1}::RFP]</i>	This study
UD676	<i>anc-1(e1873) I; [P_{col-10}::mitoLS::GFP, P_{odr-1}::RFP]</i>	This study
LIU2	<i>ldrls2 [mdt-28p::mdt-28::mCherry + unc-76(+)]</i>	Na et al., 2015
UD681	<i>anc-1(e1873) I; ldrls2</i>	This study
UD728	<i>anc-1(yc94[gfp::anc-1b::Δtk]) I</i>	This study
UD789	<i>anc-1(yc106[gfp::anc-1b::Δkash]) I</i>	This study
UD756	<i>ycSi2[pSL845 P_{y37a1b.5}::mKate2::tram-1::tram-1 3'UTR] IV</i>	This study
NM5179	<i>jsTi1493[LoxP::mex-5p::FLP:SL2::mNeonGreen::rpl-28p::FRT::GFP::his-58::FRT3] IV</i>	Nonet, 2020
UD778	<i>anc-1(yc68[gfp::anc-1b]) I; ycSi2</i>	This study
UD779	<i>anc-1(yc90[anc-1::gfp::F2]) I; ycSi2</i>	This study
UD780	<i>anc-1(yc70[gfp::anc-1b::Δ6rps]) I; ycSi2</i>	This study
UD781	<i>anc-1(yc106[gfp::anc-1b::Δkash]) I; ycSi2</i>	This study
UD782	<i>anc-1(yc94[gfp::anc-1b::Δtk]) I; ycSi2</i>	This study
UD783	<i>anc-1(yc68[gfp::anc-1b]) I; bqSi142</i>	This study
UD785	<i>anc-1(yc70[gfp::anc-1b::Δ6rps]) I; bqSi142</i>	This study
UD790	<i>anc-1(yc68[gfp::anc-1b]) I; ldrls2</i>	This study

RACE Abridged Anchor Primer and an *anc-1* specific primer: ods2574 (5'-GTCGGCGTCTGAAG-GAAAGA-3'). The PCR product was purified using the QIAquick PCR purification kit (QIAGEN) and Sanger sequencing was performed by Genewiz.

Plasmid construction and transformation

To generate plasmid *p_{anc-1b::nls::gfp::lacZ}* (pSL835), a 2.56 kb fragment of genomic DNA upstream of the start codon of *anc-1b* was amplified with primers ods2491 (5'-TACCGAGCTCAGAAAAA TGACTGTGAGTATAGTCATTTCCGCT-3') and ods2492 (5'-GTACCTTACGCTTCTTC TTTGGAGCCATTTGGTTCCGAGCAC-3') to replace the *col-19* promoter of *p_{col-19::gfp::lacZ}* (pSL779) (Cain et al., 2018). N2 animals were injected with 45 ng/μl of pSL835, 50 ng/μl of pBlue-script SK, and 2.5 ng/μl of pCFJ90 (*p_{myo-2}::mCherry*) (Frøkjær-Jensen et al., 2008) by standard *C. elegans* germline transformation (Evans, 2006) to make strain UD608 (*ycEx260[Panc-1b::nls::gfp::lacZ-2]*). Plasmid *P_{col-10}::mitoLS::gfp* (pSL289) and the *odr-1::rfp* co-injection marker were injected into N2 young adults to generate UD3 *ycEx217[P_{col-10}::mitoLS::GFP, P_{odr-1}::RFP]* transgenic strain. Flp Recombinase-Mediated Cassette Exchange (RMCE) method was used to generate strain UD756 *ycSi2[pSL845 P_{y37a1b.5}::mKate2::tram-1::tram-13'UTR]* (Nonet, 2020). pLF3FShC was a gift from Michael Nonet (Addgene plasmid # 153083; <http://n2t.net/addgene:153083>; RRID:Addgene_153083). To generate plasmid pSL845, the *P_{y37a1b.5}::mKate2* fragment amplified from pSL843 (primers: ods2785 and ods2787) and the *tram-1* fragment amplified from the *C. elegans* genomic DNA (primers: ods2788 and ods2789) were inserted into plasmid pLF3FShC through Sap I Golden Gate Assembly (Nonet, 2020).

Primers sequences are:

ods2785: 5'-CCGTAAGCTCTTCGTGGGTTGCAGAAAAATATTTCACTGTTTC-3';
ods2787: 5'-GCAACAGCTCTTCGCTCCGGAACCTCCACGGTGTCCGAGCTTGGGA-3';
ods2788 5'-GCAACAGCTCTTCGGAGGTGGATCTGGAGGTGTTAAGCCGCAAGGAGG-3';
ods2789: 5'-GCAACAGCTCTTCGTACATGTAATAAAAATATAAGAAAACGCTG-3'.

CRISPR/Cas9 mediated gene editing

Knock-in strains were generated using a *dpy-10* Co-CRISPR strategy (Arribere et al., 2014; Paix et al., 2015; Paix et al., 2017). All crRNA and repair template sequences are in Table 2. An injection mix containing 0.12 μ l *dpy-10* crRNA (0.6 mM) (Horizon Discovery/Dharmacon), 0.3 μ l target gene crRNA (0.6 mM) for one locus editing or 0.21 μ l of each crRNA (0.6 mM) for multi-loci editing and 1.46 μ l (one locus) or 1.88 μ l (two loci) universal tracrRNA (0.17 mM) (Horizon Discovery/Dharmacon) precomplexed with purified 7.6 μ l of 40 μ M Cas9 protein (UC Berkeley QB3) and 0.29 μ l of the *dpy-10* single-strand DNA oligonucleotide (ssODN) (500 ng/ μ l) repair templates and 0.21 μ l ssODN repair template (25 μ M) for the target gene editing or up to 500 ng double-strand DNA were injected to the germline of the hermaphrodite young adults. For *anc-1(yc52[Δ 25KASH]) I*, *anc-1(yc69[Δ 29KASH]) I*, *anc-1(yc62[Δ F1]) I*, *anc-1(yc61[Δ 6RPS]) I*, *anc-1(yc80[Δ F2]) I*, *anc-1(yc78[Δ 5RPS]) I*, *anc-1(yc91[gfp::anc-1b:: Δ 5rps]) I*, *anc-1(yc70[gfp::anc-1b:: Δ 6rps]) I*, *anc-1(yc92[gfp::anc-1b:: Δ f1]) I*, *anc-1(yc93[anc-1A1972,973**::gfp]) I*, *anc-1(yc106[gfp::anc-1b:: Δ kash]) I*, *anc-1(yc94[gfp::anc-1b:: Δ tk]) I* single-strand DNA (SSD) (synthesized by Integrated DNA Technologies, IDT) was used as repair template. For GFP knock-in strains, double-strand DNA repair templates were amplified with PCR from the plasmids pSL779 for *gfp* using Phusion polymerase and the primers listed in Table 2 (New England Biolabs) (Bone et al., 2016; Cain et al., 2018).

Strains *anc-1[yc41(anc-1::gfp3Xflg::kash, Δ ch)]* and *anc-1[yc36(anc-1::gfp3Xflg::kash)]* were generated by Dickinson Self-Excising Drug Selection Cassette (SEC) method (Dickinson et al., 2015). In *anc-1[yc41(anc-1::gfp3Xflg::kash, Δ ch)]*, both CH domains were deleted (starting with 23KAQK26 and ending with 322QFVR325) and replaced with GFP flanked with 9-residue long linkers (GASGASGAS).

Microscopy and imaging analysis

Images of the nuclear anchorage, worm body size measurements and *anc-1b* promoter reporter assays were collected with a wide-field epifluorescent Leica DM6000 microscope with a 63 \times Plan Apo 1.40 NA objective, a Leica DC350 FX camera, and Leica LAS AF software. ANC-1 subcellular localization, the ER marker, and nuclear shape images were taken with a spinning disc confocal microscope (Intelligent Imaging Innovations) with a CSU-X1 scan head (Yokogawa), a Cascade QuantEM 512SC camera (Photometrics), a 100 \times NA 1.46 objective (Zeiss or Nikon), and SlideBook software (Intelligent Imaging Innovations). The contrast and levels of the images were uniformly adjusted using ImageJ (National Institutes of Health). Live GFP::KDEL images were acquired at 200 ms or 250 ms intervals using the above spinning disc confocal system. To quantify ER, lipid droplet, and mitochondria positioning defects, images from at least 10 young adults of each strain were scored blindly by three people. In addition, the 'Manual Tracking' plug-in for ImageJ (<https://imagej.nih.gov/ij/plugins/track/track.html>) was used to track the positions of multiple ER fragments and lipid droplets through a time-lapse series. The relative movements between three different spots per animal were measured over time.

To quantify the fluorescent intensity of GFP::ANC-1B and GFP::ANC-1(Δ 6RPs), images were taken under the spinning disc confocal system (100X objective) and the RawIntDen of the was hypodermal area measured by ImageJ. The average fluorescent intensity was calculated by dividing the RawIntDen by the area.

For the ER colocalization analysis, z stack images were taken under the spinning disc confocal system (100X objective) and processed by background subtraction with rolling ball radius of 50.0 pixels. A Region of interest (ROI) of 96 \times 96 pixels in the non-nuclear region was cropped to use ScatterJ plugin for co-localization analysis (Zeitvogel et al., 2016).

For some adult animals, Image J 'Stitching' Plug-in was used to stitch images with overlap (Preibisch et al., 2009). The length of L2 larvae, width and length of the adult animals, as well as the circularity and solidity of the nuclei were measured with Image J.

Table 2. crRNA and repair templates used in this study.

New alleles	Strain	crRNA *	DNA repair template * †,§, ‡
<i>anc-1(yc52[Δ25KASH]) I</i>	N2	CAGUACUCGUCC UCGCAAUG	GCACTGCTTGTCTACTTATGGGAGCCGCTTGTGGTTCCACA cTgtGAtGAtGAaTAtTAATCTTTAATTTTTTATTTCATTACTATT CACTATTGTTTCATTCATCATGAACCTG
<i>anc-1(yc69[Δ29KASH]) I</i>	N2	CAGUACUCGUCC UCGCAAUG	NHEJ ‡
<i>anc-1(yc41[anc-1::gfp3Xflag::kash,Δch]) I</i>	N2	UUUCAUC UUGAAGAGGUUCG	–AAAATCTATTTTGAAAATTTTCAGATGAGGACGAG<EGFP- 3xFLAG > AGATCAGGAGCTAGCGGAGCCATGTTCCGGAGAAAGATCACCAATG–
<i>anc-1(yc62[ΔF1]) I</i>	N2	ACUUGAUCAAUCUA UAAUAA	GAAACATGAAAGCAAAGTACATTTTTTTAAAAATCGATT ATTTTCagATcGAcCAgGTACAGTCTGAGATCGACTCTTT CAGACTTCGAGGAGATCGAGCGTGAATAAACGGCTC ACTCGAAGCTTTTGAAGCCGAG
<i>anc-1(yc61[Δ6RPS]) I</i>	N2	GCGUUCAAUUUC UUCAAAU UGUUAGUA UUGGCGGCGAGU GGAGCGUUUUG UAAAAGCAA	AAGGTACAAAACATTGGAAAAACATCGATTGACGACG TGAATGTATCTGACTTCGAGGAGATCGAGCGTGAGAT CAATGGCTCCCTTGAGGCTTTCTCTATTTGGGAACG CTTCGTCAAGGCTAAAGATGATTTGTACGATTATTTG GAGAAATTAGAGAACAATGTAAGC
<i>anc-1(yc80[ΔF2]) I</i>	N2	GGAGCGUUUUG UAAAAGCAA UCCAACGGGAUC UUUGUCGU	ACTCTTATCCGGACCTTGAAGAAAGAGCTTCTATTTG GGAGCGTACTGCTTTGCCACTTCAGTGTGTT TATATTTTTTAATTAATA
<i>anc-1(yc36[anc-1::gfp3Xflag::kash]) I</i>	N2	GACAAAGATCCCG TTGGAGA	TCCGACGACA _g AGATCtCGcTGcGcCGcGTA _{CTCA} GA _{ACTTCAGGAGCTAGCGGAGCC} < EGFP- 3xFLAG > tcaggagctagcggagccGCTTTGCCACTTCAGgtttgttatatTTTT
<i>anc-1([yc68[gfp::anc-1b]]) I</i>	N2	CCGUCGGAACAGC UCCAUUU	TCTTAACCTTTTGTCCATTCACTAATTATTTTCAAT TACAGGAGGTTGGCCCGAGTCCGGTCAGTAAATTA TCAGCTGCAGTTGACGATCGATACATCTACACGTT ACACGTGCTCCGA _{ACTAAG} < EGFP > GGAGTTCCG GAGGTGGATCTGGAGGTGA _{ACTcTtCGtCGtCTGCAA} AACTTTTGGCAGCGCTGTCA _{AAAAATATTGCGATCGCAAAA} TACCA _{AAATGGAACGGAATCAAGATTTGCGAGGTTTGT} TTCA _{AAAAGCATCACA} AAATTAGCGG
<i>anc-1(yc78[Δ5RPS]) I</i>	N2	GGAGCGUUUUG UAAAAGCAA UUCCUCUGGCUU- CAACGAGU	GATCAGCTCAAGTCGGACGATTTGAAGACGGCAGAA AAGGAAATCACTAA _{tagccTcAAaCCcGAaTCTATTTGG} GA _{aAaGaTTcGTtAAgGcTAAAGATGATTTGTACGATT} ATTTGGAGAAATTAGAGAACAAT
<i>anc-1(yc90[anc-1::gfp::F2]) I</i>	N2	GGAGCGUUUUG UAAAAGCAA	CCGACCTTGAAGAAAGAGCTTCTATTTGGGAGCG TGGTGGAAAGTGGTGGAGGAAGCGGTGGA < EGFP > GCATGGATGA _{ACTATACA} AAGGAGGTTCCGGAGGTGG ATCTGGAGGTTTcGTcAAgGcTAAAGATGATTTGTACG ATTTATTTGGAGAAATTAGAGAACA
<i>anc-1(yc70[gfp::anc-1b::Δ6rps]) I</i>	UD612	GCGUUCAAUUUC UUCAAAU UGUUAGUA UUGGCGGCGAGU GGAGCGUUUUG UAAAAGCAA	AAGGTACAAAACATTGGAAAAACATCGATTGACGAC GTGAATGTATCTGACTTCGAGGAGATCGAGCGTGA GATCAATGGCTCCCTTGAGGCTTTCTCTATTTGGGA ACGCTTcGTcAAgGcTAAAGATGATTTGTACGATTAT TTGGAGAAATTAGAGAACAATGTAAGC
<i>anc-1(yc91[gfp::anc-1b::Δ5rps]) I</i>	UD612	GGAGCGUUUUG UAAAAGCAA UUCCUCUGGCUU- CAACGAGU	GATCAGCTCAAGTCGGACGATTTGAAGACGGCAGAA AAAGGAAATCACTAA _{tagccTcAAaCCcGAaTCTATTT} GGGA _{aAaGaTTcGTtAAgGcTAAAGATGATTTGTAC} GATTATTTGGAGAAATTAGAGAACAAT
<i>anc-1(yc92[gfp::anc-1b::Δf1]) I</i>	UD612	ACUUGAUCAAUCUA UAAUAA	GAAACATGAAAGCAAAGTACATTTTTTTAAAAATCG ATTATTTTCagATcGAcCAgGTACAGTCTGAGATCGAC ACTCTTTCAGACTTCGAGGAGATCGAGCGTGA _{AAAT} AAACGGCTCACTCGAAGCTTTTGAAGCCGAG
<i>anc-1(yc93[anc-1A1972,973**::gfp]) I</i>	UD612	ACUCACCUUAGAAA UUCGA	CAAAATTTAGAGCTCAGCAATGAGCAGGACTGTCC AGAT _{taatgaGgtaccCTAGAGGTGAGTATAGTCA} TTTTCCGCTCATTACACTCTT
<i>anc-1(yc71[ΔTK]) I</i>	N2	CAGAACUGC UUUGCCACUUC AUUAAAGAUUAAAA UGGUGG	GAACAACCTCCGACGACAAAGATCCCGTTGGAGACG GGTACTCAGATAATCTTTAATTTTTTATTTTCATT ACTATTCATTATTGTTTCATTCATC

Table 2 continued on next page

Table 2 continued

New alleles	Strain	crRNA *	DNA repair template * †, §, ‡
<i>anc-1(yc106[gfp::anc-1b::Δkash]) I</i>	UD612	CAGUACUCGUCG UCGCAAUG	GCACTGCTTGTCTACTTATGGGAGCCGCTTGTT TGGTTCCACAcTgTgAtGAtGaaTAtTAATCTTTAAT TTTTTATTTTCATTACTATTCACTATTGTTTCATTCATGAACCTG
<i>anc-1(yc94[gfp::anc-1b::Δtk])</i>	UD612	CAGAACUGC UUUGCCACUUC AUUAAAGAUUAAAA UGGUGG	GAACAACCTCCGACGACAAAGATCCCGTTGGAGAC GGGTACTCAGATAATCTTTAATTTTTTATTTTCA TTACTATTCACTATTGTTTCATTCATC
<i>anc-1(yc73[gfp::anc-1b::Δ6rps::Δtk]) I</i>	UD618	CAGAACUGC UUUGCCACUUC AUUAAAGAUUAAAA UGGUGG	GAACAACCTCCGACGACAAAGATCCCGTTGGAGAC GGGTACTCAGATAATCTTTAATTTTTTATTTTCA TACTATTCACTATTGTTTCATTCATC
<i>dpy-10(cn64)</i>	Co- CRISPR	GCUACCA UAGGCACCACGAG <i>Arribere et al., 2014</i>	CACTGAACTTCAATACGGCAAGATGAGAATGAC TGGAACCGTACCGCATGCGGTGCCTATGGTAGC GGAGCTTCACATGGCTTCAGACCAACAGCCTAT <i>(Arribere et al., 2014)</i>

*all nucleotide sequences are displayed as single strand in the 5' to 3' orientation.

†In many cases a ssDNA oligonucleotide was used. For larger inserts, a PCR product was used.

§An imprecise NHEJ event led to an in-frame deletion without using the repair template.

¶Underlined sequences introduce silent mutations so the repair template is not cut by Cas9.

‡Underline indicates the silent mutation in the repair template.

Statistical evaluation

The nuclear anchorage quantifying data were displayed as scatter plots with means and 95% CI as error bars. Sample sizes are indicated in the figures. The statistical tests are indicated in the figure legends. When there were limited comparisons, unpaired student t-tests were performed on the indicated comparisons for the nuclear anchorage assay, and Fisher's exact test was used. When multiple comparisons were made, ANOVA and Tukey's multiple comparisons tests were used. Prism nine software was used for the statistical analyses.

Acknowledgements

We thank Gant Luxton, Erin Cram, Charlotte Kelley, and members of the Starr lab, for helpful discussions and editing of the paper. We thank Barth Grant for sharing an unpublished strain, Erin Tapley and Yu-Tai Chang for the mitochondrial GFP strain, and Joshua Morgan for suggestions on nuclear shape measurements. We thank Michael Paddy at the MCB Light Microscopy Imaging Facility, which is a UC Davis Campus Core Research Facility, for microscopy assistance. The 3i Marianas spinning disc confocal used in this study was purchased using NIH Shared Instrumentation Grant 1S10RR024543-01. These studies were supported by the National Institutes of Health grants R01GM073874 and R35GM134859 to DAS.

Additional information

Funding

Funder	Grant reference number	Author
National Institutes of Health	R01GM073874	Daniel A Starr
National Institutes of Health	R35GM134859	Daniel A Starr

The funders had no role in study design, data collection and interpretation, or the decision to submit the work for publication.

Author contributions

Hongyan Hao, Conceptualization, Resources, Data curation, Formal analysis, Supervision, Validation, Investigation, Visualization, Methodology, Writing - original draft, Project administration, Writing - review and editing; Shilpi Kalra, Conceptualization, Formal analysis, Validation, Investigation, Methodology, Writing - review and editing; Laura E Jameson, Resources, Data curation, Formal analysis, Investigation, Writing - review and editing; Leslie A Guerrero, Natalie E Cain, Conceptualization, Resources, Formal analysis, Investigation, Methodology, Writing - review and editing; Jessica Bolivar, Conceptualization, Resources, Investigation, Methodology; Daniel A Starr, Conceptualization, Data curation, Formal analysis, Supervision, Funding acquisition, Validation, Visualization, Methodology, Writing - original draft, Project administration, Writing - review and editing

Author ORCIDs

Hongyan Hao  <https://orcid.org/0000-0003-0860-2615>

Natalie E Cain  <http://orcid.org/0000-0003-1391-404X>

Daniel A Starr  <https://orcid.org/0000-0001-7339-6606>

Decision letter and Author response

Decision letter <https://doi.org/10.7554/eLife.61069.sa1>

Author response <https://doi.org/10.7554/eLife.61069.sa2>

Additional files

Supplementary files

- Transparent reporting form

Data availability

The list of strains generated is detailed in Table 1. All data points are displayed in the histograms in the figures.

References

- Altun Z, Hall D. 2009. *Epithelial System, Hypodermis*. WormAtlas.
- Arribere JA, Bell RT, Fu BX, Artiles KL, Hartman PS, Fire AZ. 2014. Efficient marker-free recovery of custom genetic modifications with CRISPR/Cas9 in *Caenorhabditis elegans*. *Genetics* **198**:837–846. DOI: <https://doi.org/10.1534/genetics.114.169730>, PMID: 25161212
- Bone CR, Tapley EC, Gorjánác M, Starr DA. 2014. The *Caenorhabditis elegans* SUN protein UNC-84 interacts with Lamin to transfer forces from the cytoplasm to the nucleoskeleton during nuclear migration. *Molecular Biology of the Cell* **25**:2853–2865. DOI: <https://doi.org/10.1091/mbc.e14-05-0971>, PMID: 25057012
- Bone CR, Chang YT, Cain NE, Murphy SP, Starr DA. 2016. Nuclei migrate through constricted spaces using microtubule motors and actin networks in *C. elegans* hypodermal cells. *Development* **143**:4193–4202. DOI: <https://doi.org/10.1242/dev.141192>, PMID: 27697906
- Bone CR, Starr DA. 2016. Nuclear migration events throughout development. *Journal of Cell Science* **129**:1951–1961. DOI: <https://doi.org/10.1242/jcs.179788>, PMID: 27182060
- Brenner S. 1974. The genetics of *Caenorhabditis elegans*. *Genetics* **77**:71–94. PMID: 4366476
- Cain NE, Jahed Z, Schoenhofen A, Valdez VA, Elkin B, Hao H, Harris NJ, Herrera LA, Woolums BM, Mofrad MRK, Luxton GWG, Starr DA. 2018. Conserved SUN-KASH interfaces mediate LINC Complex-Dependent nuclear movement and positioning. *Current Biology* **28**:3086–3097. DOI: <https://doi.org/10.1016/j.cub.2018.08.001>, PMID: 30245107
- Calvi A, Burke B. 2015. LINC complexes and their role in human disease. *eLS* **39**:1–8. DOI: <https://doi.org/10.1042/BST20110658>
- Castiglioni VG, Pires HR, Rosas Bertolini R, Riga A, Kerver J, Boxem M. 2020. Epidermal PAR-6 and PKC-3 are essential for larval development of *C. elegans* and organize non-centrosomal microtubules. *eLife* **9**:e62967. DOI: <https://doi.org/10.7554/eLife.62067>
- Chang W, Worman HJ, Gundersen GG. 2015. Accessorizing and anchoring the LINC complex for multifunctionality. *Journal of Cell Biology* **208**:11–22. DOI: <https://doi.org/10.1083/jcb.201409047>, PMID: 25559183
- D'Alessandro M, Hnia K, Gache V, Koch C, Gavriilidis C, Rodriguez D, Nicot AS, Romero NB, Schwab Y, Gomes E, Labouesse M, Laporte J. 2015. Amphiphysin 2 orchestrates nucleus positioning and shape by linking the

- nuclear envelope to the actin and microtubule cytoskeleton. *Developmental Cell* **35**:186–198. DOI: <https://doi.org/10.1016/j.devcel.2015.09.018>, PMID: 26506308
- Davidson PM, Battistella A, Déjardin T, Betz T, Plastino J, Borghi N, Cadot B, Sykes C. 2020. Nesprin-2 accumulates at the front of the nucleus during confined cell migration. *EMBO Reports* **21**:e49910. DOI: <https://doi.org/10.15252/embr.201949910>, PMID: 32419336
- Dickinson DJ, Pani AM, Heppert JK, Higgins CD, Goldstein B. 2015. Streamlined genome engineering with a Self-Excising drug selection cassette. *Genetics* **200**:1035–1049. DOI: <https://doi.org/10.1534/genetics.115.178335>, PMID: 26044593
- Duong NT, Morris GE, Lam leT, Zhang Q, Sewry CA, Shanahan CM, Holt I. 2014. Nesprins: tissue-specific expression of epsilon and other short isoforms. *PLOS ONE* **9**:e94380. DOI: <https://doi.org/10.1371/journal.pone.0094380>, PMID: 24718612
- Elhanany-Tamir H, Yu YV, Shnyder M, Jain A, Welte M, Volk T. 2012. Organelle positioning in muscles requires cooperation between two KASH proteins and microtubules. *Journal of Cell Biology* **198**:833–846. DOI: <https://doi.org/10.1083/jcb.201204102>, PMID: 22927463
- Evans T. 2006. *The C. Elegans Research Community Transformation and Microinjection*. WormBook. DOI: <https://doi.org/10.1895/wormbook.1.108.1>
- Folker ES, Baylies MK. 2013. Nuclear positioning in muscle development and disease. *Frontiers in Physiology* **4**:363. DOI: <https://doi.org/10.3389/fphys.2013.00363>, PMID: 24376424
- Fridolfsson HN, Herrera LA, Brandt JN, Cain NE, Hermann GJ, Starr DA. 2018. Genetic analysis of nuclear migration and anchorage to study LINC complexes during development of *Caenorhabditis elegans*. *Linc Complex: Methods and Protocols* **1840**:163–180. DOI: https://doi.org/10.1007/978-1-4939-8691-0_13
- Frøkjær-Jensen C, Davis MW, Hopkins CE, Newman BJ, Thummel JM, Olesen SP, Grunnet M, Jørgensen EM. 2008. Single-copy insertion of transgenes in *Caenorhabditis elegans*. *Nature Genetics* **40**:1375–1383. DOI: <https://doi.org/10.1038/ng.248>, PMID: 18953339
- Gill NK, Ly C, Kim PH, Saunders CA, Fong LG, Young SG, Luxton GWG, Rowat AC. 2019. DYT1 dystonia Patient-Derived fibroblasts have increased deformability and susceptibility to damage by mechanical forces. *Frontiers in Cell and Developmental Biology* **7**:103. DOI: <https://doi.org/10.3389/fcell.2019.00103>, PMID: 31294022
- Gimpel P, Lee YL, Sobota RM, Calvi A, Koullourou V, Patel R, Mamchaoui K, Nédélec F, Shackleton S, Schmoranz J, Burke B, Cadot B, Gomes ER. 2017. Nesprin-1 α -Dependent microtubule nucleation from the nuclear envelope via Akap450 is necessary for nuclear positioning in muscle cells. *Current Biology* **27**:2999–3009. DOI: <https://doi.org/10.1016/j.cub.2017.08.031>
- Gonçalves JC, Quintremil S, Yi J, Vallee RB. 2020. Nesprin-2 recruitment of BicD2 to the nuclear envelope controls dynein/Kinesin-Mediated neuronal migration in Vivo. *Current Biology* **30**:3116–3129. DOI: <https://doi.org/10.1016/j.cub.2020.05.091>, PMID: 32619477
- Grady RM, Starr DA, Ackerman GL, Sanes JR, Han M. 2005. Syne proteins anchor muscle nuclei at the neuromuscular junction. *PNAS* **102**:4359–4364. DOI: <https://doi.org/10.1073/pnas.0500711102>, PMID: 15749817
- Grum VL, Li D, MacDonald RI, Mondragón A. 1999. Structures of two repeats of spectrin suggest models of flexibility. *Cell* **98**:523–535. DOI: [https://doi.org/10.1016/S0092-8674\(00\)81980-7](https://doi.org/10.1016/S0092-8674(00)81980-7), PMID: 10481916
- Gundersen GG, Worman HJ. 2013. Nuclear positioning. *Cell* **152**:1376–1389. DOI: <https://doi.org/10.1016/j.cell.2013.02.031>, PMID: 23498944
- Harris TW, Arnaboldi V, Cain S, Chan J, Chen WJ, Cho J, Davis P, Gao S, Grove CA, Kishore R, Lee RYN, Muller HM, Nakamura C, Nuin P, Paulini M, Raciti D, Rodgers FH, Russell M, Schindelman G, Auken KV, et al. 2020. WormBase: a modern model organism information resource. *Nucleic Acids Research* **48**:D762–D767. DOI: <https://doi.org/10.1093/nar/gkz920>, PMID: 31642470
- Hedgecock EM, Thomson JN. 1982. A gene required for nuclear and mitochondrial attachment in the nematode *Caenorhabditis elegans*. *Cell* **30**:321–330. DOI: [https://doi.org/10.1016/0092-8674\(82\)90038-1](https://doi.org/10.1016/0092-8674(82)90038-1), PMID: 6889924
- Holt I, Duong NT, Zhang Q, Lam leT, Sewry CA, Mamchaoui K, Shanahan CM, Morris GE. 2016. Specific localization of nesprin-1- α 2, the short isoform of nesprin-1 with a KASH domain, in developing, fetal and regenerating muscle, using a new monoclonal antibody. *BMC Cell Biology* **17**:26. DOI: <https://doi.org/10.1186/s12860-016-0105-9>, PMID: 27350129
- Jaalouk DE, Lammerding J. 2009. Mechanotransduction gone awry. *Nature Reviews Molecular Cell Biology* **10**:63–73. DOI: <https://doi.org/10.1038/nrm2597>, PMID: 19197333
- Jahed Z, Hao H, Thakkar V, Vu UT, Valdez VA, Rathish A, Tolentino C, Kim SCJ, Fadavi D, Starr DA, Mofrad MRK. 2019. Role of KASH domain lengths in the regulation of LINC complexes. *Molecular Biology of the Cell* **30**:2076–2086. DOI: <https://doi.org/10.1091/mbc.E19-02-0079>, PMID: 30995155
- Jayo A, Malboubi M, Antoku S, Chang W, Ortiz-Zapater E, Groen C, Pfisterer K, Tootle T, Charras G, Gundersen GG, Parsons M. 2016. Fascin regulates nuclear movement and deformation in migrating cells. *Developmental Cell* **38**:371–383. DOI: <https://doi.org/10.1016/j.devcel.2016.07.021>, PMID: 27554857
- Kamath RS, Ahringer J. 2003. Genome-wide RNAi screening in *Caenorhabditis elegans*. *Methods* **30**:313–321. DOI: [https://doi.org/10.1016/S1046-2023\(03\)00050-1](https://doi.org/10.1016/S1046-2023(03)00050-1), PMID: 12828945
- Kutscheidt S, Zhu R, Antoku S, Luxton GW, Stagljar I, Fackler OT, Gundersen GG. 2014. FHOD1 interaction with nesprin-2G mediates TAN line formation and nuclear movement. *Nature Cell Biology* **16**:708–715. DOI: <https://doi.org/10.1038/ncb2981>, PMID: 24880667
- Lee YL, Burke B. 2018. LINC complexes and nuclear positioning. *Seminars in Cell & Developmental Biology* **82**:67–76. DOI: <https://doi.org/10.1016/j.semdb.2017.11.008>, PMID: 29191370

- Liem RK.** 2016. Cytoskeletal integrators: the spectrin superfamily. *Cold Spring Harbor Perspectives in Biology* **8**: a018259. DOI: <https://doi.org/10.1101/cshperspect.a018259>, PMID: 27698030
- Lüke Y, Zaim H, Karakesisoglou I, Jaeger VM, Sellin L, Lu W, Schneider M, Neumann S, Beijer A, Munck M, Padmakumar VC, Gloy J, Walz G, Noegel AA.** 2008. Nesprin-2 giant (NUANCE) maintains nuclear envelope architecture and composition in skin. *Journal of Cell Science* **121**:1887–1898. DOI: <https://doi.org/10.1242/jcs.019075>, PMID: 18477613
- Luxton GW, Gomes ER, Folker ES, Vintinner E, Gundersen GG.** 2010. Linear arrays of nuclear envelope proteins harness retrograde actin flow for nuclear movement. *Science* **329**:956–959. DOI: <https://doi.org/10.1126/science.1189072>, PMID: 20724637
- Luxton GW, Starr DA.** 2014. KASHing up with the nucleus: novel functional roles of KASH proteins at the cytoplasmic surface of the nucleus. *Current Opinion in Cell Biology* **28**:69–75. DOI: <https://doi.org/10.1016/j.ceb.2014.03.002>, PMID: 24704701
- Mello CC, Kramer JM, Stinchcomb D, Ambros V.** 1991. Efficient gene transfer in *C. elegans*: extrachromosomal maintenance and integration of transforming sequences. *The EMBO Journal* **10**:3959–3970. DOI: <https://doi.org/10.1002/j.1460-2075.1991.tb04966.x>, PMID: 1935914
- Morales-Martínez A, Dobrzynska A, Askjaer P.** 2015. Inner nuclear membrane protein LEM-2 is required for correct nuclear separation and morphology in *C. elegans*. *Journal of Cell Science* **128**:1090–1096. DOI: <https://doi.org/10.1242/jcs.164202>, PMID: 25653391
- Na H, Zhang P, Chen Y, Zhu X, Liu Y, Liu Y, Xie K, Xu N, Yang F, Yu Y, Cichello S, Mak HY, Wang MC, Zhang H, Liu P.** 2015. Identification of lipid droplet structure-like/resident proteins in *Caenorhabditis elegans*. *Biochimica Et Biophysica Acta (BBA) - Molecular Cell Research* **1853**:2481–2491. DOI: <https://doi.org/10.1016/j.bbamcr.2015.05.020>
- Nonet ML.** 2020. Efficient transgenesis in *Caenorhabditis elegans* Using Flp Recombinase-Mediated Cassette Exchange. *Genetics* **215**:903–921. DOI: <https://doi.org/10.1534/genetics.120.303388>, PMID: 32513816
- Ostlund C, Folker ES, Choi JC, Gomes ER, Gundersen GG, Worman HJ.** 2009. Dynamics and molecular interactions of Linker of nucleoskeleton and cytoskeleton (LINC) complex proteins. *Journal of Cell Science* **122**:4099–4108. DOI: <https://doi.org/10.1242/jcs.057075>, PMID: 19843581
- Paix A, Folkmann A, Rasoloson D, Seydoux G.** 2015. High efficiency, Homology-Directed genome editing in *Caenorhabditis elegans* using CRISPR-Cas9 ribonucleoprotein complexes. *Genetics* **201**:47–54. DOI: <https://doi.org/10.1534/genetics.115.179382>, PMID: 26187122
- Paix A, Folkmann A, Seydoux G.** 2017. Precision genome editing using CRISPR-Cas9 and linear repair templates in *C. elegans*. *Methods* **121-122**:86–93. DOI: <https://doi.org/10.1016/j.ymeth.2017.03.023>
- Potter C, Zhu W, Razafsky D, Ruzycski P, Kolesnikov AV, Doggett T, Kefalov VJ, Betleja E, Mahjoub MR, Hodzic D.** 2017. Multiple isoforms of Nesprin1 are integral components of ciliary rootlets. *Current Biology* **27**:2014–2022. DOI: <https://doi.org/10.1016/j.cub.2017.05.066>
- Preibisch S, Saalfeld S, Tomancak P.** 2009. Globally optimal stitching of tiled 3D microscopic image acquisitions. *Bioinformatics* **25**:1463–1465. DOI: <https://doi.org/10.1093/bioinformatics/btp184>, PMID: 19346324
- Rajgor D, Mellad JA, Autore F, Zhang Q, Shanahan CM.** 2012. Multiple novel nesprin-1 and nesprin-2 variants act as versatile tissue-specific intracellular scaffolds. *PLOS ONE* **7**:e40098. DOI: <https://doi.org/10.1371/journal.pone.0040098>, PMID: 22768332
- Rajgor D, Shanahan CM.** 2013. Nesprins: from the nuclear envelope and beyond. *Expert Reviews in Molecular Medicine* **15**:e5. DOI: <https://doi.org/10.1017/erm.2013.6>, PMID: 23830188
- Ralston E, Lu Z, Biscocho N, Soumaka E, Mavroidis M, Prats C, Lømo T, Capetanaki Y, Ploug T.** 2006. Blood vessels and desmin control the positioning of nuclei in skeletal muscle fibers. *Journal of Cellular Physiology* **209**:874–882. DOI: <https://doi.org/10.1002/jcp.20780>, PMID: 16972267
- Rolls MM, Hall DH, Victor M, Stelzer EH, Rapoport TA.** 2002. Targeting of rough endoplasmic reticulum membrane proteins and ribosomes in invertebrate neurons. *Molecular Biology of the Cell* **13**:1778–1791. DOI: <https://doi.org/10.1091/mbc.01-10-0514>, PMID: 12006669
- Roman W, Gomes ER.** 2018. Nuclear positioning in skeletal muscle. *Seminars in Cell & Developmental Biology* **82**:51–56. DOI: <https://doi.org/10.1016/j.semcdb.2017.11.005>, PMID: 29241690
- Roux KJ, Crisp ML, Liu Q, Kim D, Kozlov S, Stewart CL, Burke B.** 2009. Nesprin 4 is an outer nuclear membrane protein that can induce kinesin-mediated cell polarization. *PNAS* **106**:2194–2199. DOI: <https://doi.org/10.1073/pnas.0808602106>, PMID: 19164528
- Starr DA.** 2019. A network of nuclear envelope proteins and cytoskeletal force generators mediates movements of and within nuclei throughout *Caenorhabditis elegans* development. *Experimental Biology and Medicine* **244**:1323–1332. DOI: <https://doi.org/10.1177/1535370219871965>
- Starr DA, Fridolfsson HN.** 2010. Interactions between nuclei and the cytoskeleton are mediated by SUN-KASH nuclear-envelope bridges. *Annual Review of Cell and Developmental Biology* **26**:421–444. DOI: <https://doi.org/10.1146/annurev-cellbio-100109-104037>, PMID: 20507227
- Starr DA, Han M.** 2002. Role of ANC-1 in tethering nuclei to the actin cytoskeleton. *Science* **298**:406–409. DOI: <https://doi.org/10.1126/science.1075119>, PMID: 12169658
- Stewart-Hutchinson PJ, Hale CM, Wirtz D, Hodzic D.** 2008. Structural requirements for the assembly of LINC complexes and their function in cellular mechanical stiffness. *Experimental Cell Research* **314**:1892–1905. DOI: <https://doi.org/10.1016/j.yexcr.2008.02.022>, PMID: 18396275
- Stroud MJ, Feng W, Zhang J, Veevers J, Fang X, Gerace L, Chen J.** 2017. Nesprin 1 α 2 is essential for mouse postnatal viability and nuclear positioning in skeletal muscle. *Journal of Cell Biology* **216**:1915–1924. DOI: <https://doi.org/10.1083/jcb.201612128>, PMID: 28533284

- Terns RM**, Kroll-Conner P, Zhu J, Chung S, Rothman JH. 1997. A deficiency screen for zygotic loci required for establishment and patterning of the epidermis in *Caenorhabditis elegans*. *Genetics* **146**:185–206. DOI: <https://doi.org/10.1093/genetics/146.1.185>, PMID: 9136010
- Thompson O**, Edgley M, Strasbourger P, Flibotte S, Ewing B, Adair R, Au V, Chaudhry I, Fernando L, Hutter H, Kieffer A, Lau J, Lee N, Miller A, Raymant G, Shen B, Shendure J, Taylor J, Turner EH, Hillier LW, et al. 2013. The million mutation project: a new approach to genetics in *Caenorhabditis elegans*. *Genome Research* **23**: 1749–1762. DOI: <https://doi.org/10.1101/gr.157651.113>, PMID: 23800452
- Timmons L**, Fire A. 1998. Specific interference by ingested dsRNA. *Nature* **395**:854. DOI: <https://doi.org/10.1038/27579>, PMID: 9804418
- Tsujikawa M**, Omori Y, Biyanwila J, Malicki J. 2007. Mechanism of positioning the cell nucleus in vertebrate photoreceptors. *PNAS* **104**:14819–14824. DOI: <https://doi.org/10.1073/pnas.0700178104>, PMID: 17785424
- van Bergeijk P**, Hoogenraad CC, Kapitein LC. 2016. Right time, right place: probing the functions of organelle positioning. *Trends in Cell Biology* **26**:121–134. DOI: <https://doi.org/10.1016/j.tcb.2015.10.001>, PMID: 26541125
- Waaijers S**, Muñoz J, Berends C, Ramalho JJ, Goerdal SS, Low TY, Zoumaro-Djajoon AD, Hoffmann M, Koorman T, Tas RP, Harterink M, Seelk S, Kerver J, Hoogenraad CC, Bossinger O, Tursun B, van den Heuvel S, Heck AJ, Boxem M. 2016. A tissue-specific protein purification approach in *Caenorhabditis elegans* identifies novel interaction partners of DLG-1/Discs large. *BMC Biology* **14**:66. DOI: <https://doi.org/10.1186/s12915-016-0286-x>, PMID: 27506200
- Wang N**, Tytell JD, Ingber DE. 2009. Mechanotransduction at a distance: mechanically coupling the extracellular matrix with the nucleus. *Nature Reviews Molecular Cell Biology* **10**:75–82. DOI: <https://doi.org/10.1038/nrm2594>, PMID: 19197334
- Wang S**, Reuveny A, Volk T. 2015. Nesprin provides elastic properties to muscle nuclei by cooperating with spectraplakins and EB1. *Journal of Cell Biology* **209**:529–538. DOI: <https://doi.org/10.1083/jcb.201408098>, PMID: 26008743
- Xu D**, Zhang Y. 2012. Ab initio protein structure assembly using continuous structure fragments and optimized knowledge-based force field. *Proteins: Structure, Function, and Bioinformatics* **80**:1715–1735. DOI: <https://doi.org/10.1002/prot.24065>, PMID: 22411565
- Xu D**, Zhang Y. 2013. Toward optimal fragment generations for ab initio protein structure assembly. *Proteins* **81**: 229–239. DOI: <https://doi.org/10.1002/prot.24179>, PMID: 22972754
- Zeitvogel F**, Schmid G, Hao L, Ingino P, Obst M. 2016. ScatterJ: an ImageJ plugin for the evaluation of analytical microscopy datasets. *Journal of Microscopy* **261**:148–156. DOI: <https://doi.org/10.1111/jmi.12187>, PMID: 25515182
- Zhang Q**, Skepper JN, Yang F, Davies JD, Hegyi L, Roberts RG, Weissberg PL, Ellis JA, Shanahan CM. 2001. Nesprins: a novel family of spectrin-repeat-containing proteins that localize to the nuclear membrane in multiple tissues. *Journal of Cell Science* **114**:4485–4498. PMID: 11792814
- Zheng Y**, Buchwalter RA, Zheng C, Wight EM, Chen JV, Megraw TL. 2020. A perinuclear microtubule-organizing centre controls nuclear positioning and basement membrane secretion. *Nature Cell Biology* **22**:297–309. DOI: <https://doi.org/10.1038/s41556-020-0470-7>, PMID: 32066907